

Research Article: New Research | Sensory and Motor Systems

Perturbations of Respiratory Rhythm and Pattern by Disrupting Synaptic Inhibition within Pre-Bötzinger and Bötzing Complexes

Role of synaptic inhibition in pre-BötC and BötC

Vitaliy Marchenko^{1,*}, Hidehiko Koizumi^{2,*}, Bryan Mosher², Naohiro Koshiya², Mohammad F. Tariq², Tatiana G. Bezdudnaya¹, Ruli Zhang², Yaroslav I. Molkov³, Ilya A. Rybak¹ and Jeffrey C. Smith²

¹*Department of Neurobiology and Anatomy, Drexel University College of Medicine, Philadelphia, Pennsylvania 19129*

²*Cellular and Systems Neurobiology Section, National Institute of Neurological Disorders and Stroke, National Institutes of Health, Bethesda, Maryland 20892*

³*Department of Mathematics and Statistics, Georgia State University, Atlanta, Georgia 30302*

DOI: 10.1523/ENEURO.0011-16.2016

Received: 16 January 2016

Revised: 15 April 2016

Accepted: 18 April 2016

Published: 2 May 2016

Author contributions: V.M., H.K., I.A.R., and J.C.S. designed research; V.M., H.K., B.M., T.B., and R.Z. performed research; H.K., N.K., M.F.T., R.Z., and Y.I.M. analyzed data; I.A.R. and J.C.S. wrote the paper.

Funding: NIH: R01 NS069220. NIH: R01 AT008632. NIH/NINDS;

Conflict of Interest: Authors report no conflict of interest.

Intramural Research Program of NIH/NINDS, and NIH grants R01 NS069220 and R01 AT008632.

*These authors contributed equally to this study

Correspondence should be addressed to: Jeffrey C. Smith, Ph.D., 49 Convent Drive, Room 2A10, NINDS, NIH, Bethesda, MD 20892. Tel. (301) 496-4960. FAX: (301) 496-1339. Email: smithj2@helix.nih.gov

Cite as: eNeuro 2016; 10.1523/ENEURO.0011-16.2016

Alerts: Sign up at eneuro.org/alerts to receive customized email alerts when the fully formatted version of this article is published.

Accepted manuscripts are peer-reviewed but have not been through the copyediting, formatting, or proofreading process.

This is an open-access article distributed under the terms of the Creative Commons Attribution 4.0 International (<http://creativecommons.org/licenses/by/4.0>), which permits unrestricted use, distribution and reproduction in any medium provided that the original work is properly attributed.

- 1 1. Manuscript Title:
2
3 **Perturbations of Respiratory Rhythm and Pattern by Disrupting Synaptic Inhibition**
4 **within Pre-Bötzinger and Bötzing Complexes**
5
- 6 2. Abbreviated Title:
7
8 **Role of synaptic inhibition in pre-BötC and BötC**
9
- 10 3. List all Author Names and Affiliations in order as they would appear in the published article:
11
12 **Vitaliy Marchenko^{1*}, Hidehiko Koizumi^{2*}, Bryan Mosher², Naohiro Koshiya²,**
13 **Mohammad F. Tariq², Tatiana G. Bezdudnaya¹, Ruli Zhang², Yaroslav I. Molkov³,**
14 **Ilya A. Rybak¹, and Jeffrey C. Smith²**
15
- 16 ¹**Department of Neurobiology and Anatomy, Drexel University College of Medicine,**
17 **Philadelphia, Pennsylvania 19129**
18 ²**Cellular and Systems Neurobiology Section, National Institute of Neurological Disorders**
19 **and Stroke, National Institutes of Health, Bethesda, Maryland 20892**
20 ³**Department of Mathematics and Statistics, Georgia State University, Atlanta, Georgia**
21 **30302**
22
- 23 *** These authors contributed equally to this study**
24
- 25 4. Author Contributions:
26
27 **J.C.S., I.A.R., H.K. and V.M. designed research;**
28 **V.M., H.K., B.M., R.Z., and T.G.B. performed research;**
29 **Y.I.M., N.K., H.K., M.F.T., and R.Z. analyzed data;**
30 **J.C.S. and I.A.R. wrote the paper.**
31
- 32 5. Correspondence should be addressed to:
33
34 **Jeffrey C. Smith, Ph.D.**
35 **49 Convent Drive, Room 2A10**
36 **NINDS, NIH, Bethesda, MD 20892**
37 **Tel. (301) 496-4960**
38 **FAX: (30) 496-1339**
39 **Email: smithj2@helix.nih.gov**
40
- | | | |
|-----------------------------------|--|-------------|
| 6. Number of Figures: 14 | 9. Number of words for Abstract | 249 |
| 7. Number of Tables: 0 | 10. Number of words for Significance Statement | 120 |
| 8. Number of Multimedia: 0 | 11. Number of words for Introduction | 763 |
| | 12. Number of words for Discussion | 3204 |
- 41 13. Acknowledgements
42
43 **This study was supported in part by the Intramural Research Program of the National**
44 **Institutes of Health (NIH), National Institute of Neurological Disorders and Stroke, and**
45 **NIH grants R01 NS069220 and R01 AT008632**
46
- 47 14. Conflict of Interest:
48
49 **The authors declare no competing financial interests**
50
- 51 15. Funding sources:
52 **Intramural Research Program of NIH/NINDS, and NIH grants R01 NS069220 and R01 AT008632**

53 **Perturbations of Respiratory Rhythm and Pattern by Disrupting**
54 **Synaptic Inhibition within Pre-Bötzinger and Bötzinger Complexes**

55 **Abstract**

56 The pre-Bötzinger (pre-BötC) and Bötzinger (BötC) complexes are the brainstem compartments
57 containing interneurons considered to be critically involved in generating respiratory rhythm and
58 motor pattern in mammals. Current models postulate that both generation of the rhythm and
59 coordination of the inspiratory-expiratory pattern involve inhibitory synaptic interactions within
60 and between these regions. Both regions contain glycinergic and GABAergic neurons, and
61 rhythmically active neurons in these regions receive appropriately coordinated phasic inhibition
62 necessary for generation of the normal three-phase respiratory pattern. However, recent
63 experiments attempting to disrupt glycinergic and GABAergic postsynaptic inhibition in the pre-
64 BötC and BötC in adult rats *in vivo* have questioned the critical role of synaptic inhibition in
65 these regions as well as the importance of the BötC, which contradicts previous physiological
66 and pharmacological studies. To further evaluate the roles of synaptic inhibition and the BötC,
67 we bilaterally microinjected the GABA_A receptor antagonist gabazine and glycinergic receptor
68 antagonist strychnine into the pre-BötC or BötC in anesthetized adult rats *in vivo* and in perfused
69 *in situ* brainstem-spinal cord preparations from juvenile rats. Muscimol was microinjected to
70 suppress neuronal activity in the pre-BötC or BötC. In both preparations, disrupting inhibition
71 within pre-BötC or BötC caused major site-specific perturbations of the rhythm and disrupted the
72 three-phase motor pattern, in some experiments terminating rhythmic motor output. Suppressing
73 BötC activity also potently disturbed the rhythm and motor pattern. We conclude that inhibitory
74 circuit interactions within and between the pre-BötC and BötC critically regulate rhythmogenesis
75 and are required for normal respiratory motor pattern generation.

76 **Significance Statement**

77 Defining functional roles of postsynaptic inhibition in respiratory and other mammalian central
78 pattern generation circuits is a longstanding problem. Inhibitory circuit interactions within and
79 between the brainstem respiratory pre-BötC and BötC have been proposed to be critically
80 involved in normal rhythm and motor pattern generation. A fundamental role of postsynaptic
81 inhibition in these regions has been questioned in recent experiments attempting to
82 pharmacologically disrupt this inhibition. To resolve this contradiction, we applied similar
83 approaches of microinjecting selective pharmacological antagonists of GABA_Aergic and
84 glycinergic receptor-mediated inhibition in the pre-BötC and BötC in rats. Our results
85 demonstrate large, site-specific perturbations of respiratory rhythm and motor pattern including
86 disruption of rhythmic motor output and thus confirm the critical role of inhibitory circuit
87 interactions.

88

89 Introduction

90 Rhythmic movements such as breathing and locomotion are produced by central pattern
91 generator (CPG) networks containing interacting excitatory and inhibitory circuits. These circuits
92 are the neural substrates for producing motor behavior (Grillner, 2006) and defining their
93 specific roles in rhythmic motor pattern generation is key to understanding the functional
94 operation of CPGs. Here we have addressed the longstanding problem of defining roles of
95 inhibitory circuits in core structures of the mammalian brainstem respiratory CPG.

96 The respiratory neural pattern under normal conditions includes three phases: inspiration,
97 post-inspiration and late expiration (Richter, 1996; Richter and Smith, 2014). The kernel of the
98 respiratory CPG located in the ventral respiratory column (VRC) of the medulla includes two
99 key compartments, the pre-Bötzinger (pre-BötC) and Bötzinger (BötC) complexes (Alheid and
100 McCrimmon, 2008; Smith et al., 2009, 2013). The pre-BötC contains a heterogeneous population
101 of excitatory neurons, including cells with intrinsic bursting properties, and excitatory synaptic
102 interconnections that generate rhythmic inspiratory activity and drive inspiratory motor output.
103 This excitatory population, when isolated in slices *in vitro*, generates inspiratory bursting activity
104 (Smith et al., 1991; Koshiya and Smith, 1999) that persists after disrupting synaptic inhibition
105 (Johnson et al., 2001). In addition, the pre-BötC contains GABAergic and glycinergic neuron
106 populations (Kuwana et al., 2006; Winter et al., 2009; Morgado-Valle et al., 2010; Koizumi et al.,
107 2013) providing phasic inspiratory inhibition widely distributed in the brainstem including
108 inhibition of BötC expiratory neurons. In turn, BötC post-inspiratory and expiratory neurons
109 provide phasic expiratory inhibition (Jiang and Lipski, 1990; Tian et al., 1999a,b; Ezure et al.,
110 2003a,b) including to pre-BötC inspiratory neurons to coordinate generation of expiratory and
111 inspiratory phases.

112 The specific contributions of the intrinsic excitatory bursting mechanisms in the pre-
113 BötC, and inhibitory network interactions between pre-BötC and BötC, to respiratory rhythm and
114 motor pattern generation are not clearly understood and this issue is continuously debated. Early
115 theoretical models, based entirely on network inhibitory interactions, could not explain the
116 maintenance of rhythm after blockade of synaptic inhibition *in vitro*. Alternatively, the pure
117 autorhythmic excitatory network models, developed to explain the *in vitro* data, could not
118 account for many behaviors observed *in vivo*, such as the Hering-Breuer inspiratory inhibitory
119 and other respiratory reflexes and the coordinated generation of multiple respiratory phases.
120 Also, these models could not reproduce apneusis, a breathing pattern characterized by a
121 significantly prolonged inspiration alternating with short expiratory intervals (Lindsay et al.,
122 2012).

123 To resolve this problem, more complicated models have been developed (Rybak et al.,
124 2004, 2007; Smith et al., 2007, 2009, 2013) hypothesizing that: (i) the pre-BötC, while capable
125 of autonomous generation of rhythmic bursting when isolated *in vitro*, is embedded in the larger
126 respiratory network where its activity is controlled by interactions with other brainstem
127 compartments, including inputs from excitatory RTN/pFRG neurons, and from the inhibitory
128 neuron populations in BötC, and (ii) both the intrinsic bursting of pre-BötC inspiratory neurons
129 and inhibitory interactions between the neural populations in pre-BötC and BötC are
130 fundamentally involved in generating the normal rhythmic respiratory pattern. Disruption of
131 inhibition in these circuits would lead either to switching to the intrinsic rhythmic activity
132 originating within the pre-BötC, or to sustained or apneustic-like activity.

133 This concept was challenged by a recent study in the anesthetized rat employing targeted
134 pharmacological blockade of fast inhibitory neurotransmission (Janczewski et al., 2013) from

135 which it was concluded that (i) the BötC does not play a role in respiratory rhythm/pattern
136 generation, and (ii) inhibition within the pre-BötC and BötC is not required for generating a
137 normal breathing rhythm and pattern.

138 The present study was focused on resolving this contradiction and further evaluating roles
139 of inhibitory interactions in pre-BötC and BötC in rhythm generation and shaping respiratory
140 pattern. Our experiments were performed using two distinct preparations, the anesthetized,
141 vagotomized adult rat and the arterially perfused *in situ* brainstem-spinal cord preparation of
142 juvenile rat. Specific pharmacological blockers of glycinergic (strychnine) and GABA_Aergic
143 (gabazine) receptor-mediated inhibition were selectively microinjected into the pre-BötC or
144 BötC and perturbations of the respiratory frequency and phases were evaluated. In addition,
145 microinjections of the GABA_A receptor agonist muscimol were used to inhibit neural activity in
146 each compartment. Our results were not consistent with those reported by Janczewski et al.
147 (2013). Disrupting inhibition within pre-BötC or BötC as well as inhibiting BötC activity caused
148 major perturbations of the respiratory frequency and three-phase pattern. Moreover, blocking
149 inhibition within the BötC lead to apnea confirming the critical role of inhibitory interactions
150 between pre-BötC and BötC. Our results are consistent with previous proposals of the important
151 role of inhibitory interactions within and between pre-BötC and BötC in generating and shaping
152 the respiratory pattern.

153

154 **Materials and Methods**

155 *Animal procedures*

156 All experimental procedures used in this study were approved by either the NINDS Animal Care
157 and Use Committee, or the Drexel University Institutional Animal Care and Use Committee,
158 which oversees Drexel University's AAALAC International-accredited animal program. All
159 electrophysiological recording and pharmacological microinjection experiments were performed
160 via a surgically exposed ventral brainstem for access to the ventro-lateral medullary pre-BötC
161 and BötC regions (**Figure 1**).

162 *Surgical procedures in adult rats in vivo*

163 Spontaneously breathing, adult male Sprague-Dawley rats (340–380 g) were anesthetized with
164 isoflurane vaporized in O₂ (Matrix; 4–5% induction, 1.75–2.0% maintenance) via a snout mask.
165 Anesthetic depth was maintained at a level at which withdrawal reflexes as well as changes in
166 heart rate and blood pressure (BP) in response to pinching the distal hind limbs were absent.
167 After tracheotomy with a glass tube, animals were artificially ventilated with the same gas
168 mixture (60 min⁻¹, 2.5–3.0 ml tidal volume; Columbus Apparatus rodent ventilator).
169 Electrocardiogram (EKG) was measured via three small subcutaneous electrodes using
170 conventional amplification and filtering (Neurolog; Digitimer) and monitored using an audio
171 amplifier (model AM10; Grass Instruments) and oscilloscope (Tektronix). One femoral artery
172 and vein were cannulated for measurement of arterial pressure and infusion of drugs/saline,
173 respectively. During all surgical procedures, rectal temperature was maintained at 37.0 ± 0.1°C
174 via a servo-controlled heating blanket coupled to a rectal thermometer (Harvard Apparatus). The
175 phrenic (PN) nerve was prepared for recording by dissecting the nerves free from the

176 surrounding tissue. Ventral neck muscles (cleidomastoideus, sternomastoideus, sternohyoideus,
177 omohypides and digastricus), infrathyroid portions of the trachea and esophagus were removed.
178 The body of the 1st neck vertebra (atlas) and base portion of occipital bone were removed to
179 expose the ventral medulla and the axo-occipital membrane was cut. The dura was then opened
180 using iridectomy scissors and residual bleeding from lateral epidural sinus was arrested by
181 applying small pieces of gelfoam (USP; Pharmacia) soaked with thrombin solution ($50 \text{ U} \cdot \text{ml}^{-1}$
182 USP, Biopharm Lab) dissolved in artificial cerebrospinal fluid (aCSF).

183 All animals were vagotomized and baro- and chemoreceptor denervated via bilateral
184 transection of the carotid sinus nerves to prevent cardiorespiratory reflex influences on motor
185 nerve outputs (Richter and Seller, 1975; Grundy et al., 1986; Hopp and Seagar, 1998; Virkkia et
186 al., 2007; Baekey et al., 2010). A bilateral pneumothorax was performed before
187 electrophysiological recording to eliminate lung inflation-related movement artifacts and chest
188 wall mechanoreceptor feedback. A positive end-expiratory pressure of 1.0 cm H_2O was
189 maintained to prevent lung atelectasis during expiration. Animals were paralyzed by an
190 intravenous bolus injection (2 mg/kg), followed by continuous infusion (3–4 mg/kg/h), of
191 vecuronium bromide (Abbott Laboratories) dissolved in Ringer-Locke solution. End-tidal CO_2
192 was maintained between 5.0% and 5.5% (Capstar, CWE Inc.) by adjusting frequency of
193 ventilation. If necessary, animals were continuously infused with Ringer-Locke solution (1.0–
194 1.25% body weight or 10.0–12.5 ml/kg/h) to maintain a stable mean arterial pressure of 85–95
195 mmHg.

196 ***In situ arterially perfused brainstem-spinal cord preparation***

197 Experiments were also performed with the *in situ* arterially perfused brain-stem spinal cord
198 preparations from juvenile rats (3–5 weeks old) as previously described (Paton, 1996; Smith et

199 al., 2007). These preparations were studied because they provide the opportunity to investigate
200 roles of synaptic inhibition in an unanesthetized preparation generating the three-phase
201 respiratory pattern that could be clearly identified from simultaneous recordings of spinal and
202 cranial nerves, including prominent post-inspiratory discharge recorded from the central vagus
203 nerve (cVN). We note that cVN recordings from the normocapnic, vagotomized, carotid body
204 denervated, and isoflurane anesthetized adult rats *in vivo* in our experiments do not routinely
205 exhibit post-I discharge although neuronal recording in the BötC always shows post-I activity
206 (e.g., see Figure 3B), which is an important feature of medullary respiratory circuit activity.
207 Furthermore, a number of theoretical models (e.g., Rybak et al., 2007; Smith et al., 2007; Rubin
208 et al., 2009; Shevstova et al., 2011, 2014; Richter and Smith, 2014) postulating roles of pre-BötC
209 and BötC inhibitory circuits in respiratory rhythm and pattern generation have been based in part
210 on experimental results obtained from these *in situ* preparations. It is therefore critical to test
211 their roles in this preparation, and to compare results from the *in vivo* anesthetized adult rat
212 preparations utilizing a similar strategy for targeted disruption of synaptic inhibition in the pre-
213 BötC and BötC.

214 Preheparinized (1,000 units, given intraperitoneally) juvenile rats (Sprague-Dawley, 45–
215 90 g; male) were anaesthetized deeply with 5% isoflurane and the portion of the body caudal to
216 the diaphragm was removed. The head and thorax were immersed in ice-chilled carbogenated
217 aCSF solution (1.25 mM MgSO₄, 1.25 mM KH₂PO₄, 5.0 mM KCl, 25 mM NaHCO₃, 125 mM
218 NaCl, 2.5 mM CaCl₂, 10 mM dextrose, 0.1785 mM polyethylene glycol) and the rat was
219 decerebrated at a precollicular level. The descending aorta, PN and cervical vagus nerve (cVN)
220 were surgically isolated. As with the *in vivo* preparations, ventral neck muscles, infrathyroid
221 portions of the trachea, the esophagus, and then the 1st neck vertebra and base portion of the

222 occipital bone were removed to expose the ventral medulla. The axo-occipital membrane was
223 cut, and the dura was then cut open. The preparation was transferred to a recording chamber and
224 secured in a stereotaxic head frame ventral side up. The descending aorta was cannulated with a
225 double lumen catheter for perfusion and recording of perfusion pressure with a pressure
226 transducer (Micron Instruments). Vecuronium bromide was added to the perfusate to block
227 neuromuscular transmission (4 $\mu\text{g}/\text{ml}$; SUN Pharmaceutical Industries). The perfusate was
228 gassed with 95% O_2 / 5% CO_2 and maintained at 31 $^{\circ}\text{C}$. Vasopressin (200–400 pM as required;
229 APP Pharmaceuticals) was added to the perfusate to raise and maintain perfusion pressure
230 between 70 and 80 mmHg (Paton et al., 2006). Unless stated, all chemicals were from Sigma.

231 *Electrophysiological recording in vivo*

232 With the rat in the supine position, the central ends of the cut PN were placed on bipolar silver
233 hook electrodes for recording (10–5,000 Hz bandpass; Neurolog, Digitimer) and immersed in a
234 mineral oil pool formed by skin flaps. To identify precise locations of the BötC and pre-BötC the
235 activity of medullary expiratory and (pre)inspiratory neurons was recorded (200–3,000 Hz
236 bandpass; Neurolog) by a ventral approach and glass (WPI) microelectrodes (tip outer diameter
237 of 2–3 μm , 5–10 $\text{M}\Omega$) filled with 0.5 M NaCl and 2% pontamine sky blue. The pre-BötC is
238 readily identified by a characteristic pattern of pre-inspiratory-inspiratory (pre-I/I) activity (see
239 **Figure 3A**) and the BötC has a characteristic profile of post-inspiratory (post-I) and augmenting
240 expiratory (aug-E) activities (see **Figure 3B**). The microelectrode was held in a 3-dimensional
241 stepper motor assembly (DC-3K, Märzhäuser), attached to the rail of the stereotaxic frame, and
242 advanced in steps of 2.5–5.0 μm . After mapping neuronal activity, the medullary surface was
243 marked bilaterally by iontophoresis for 15 min. of the pontamine sky blue dye (-25 nA, 0.125 Hz,
244 4 s; Axoclamp 2A) as a guide spot for insertion of drug microinjection pipettes. All

245 electrophysiological signals were recorded simultaneously with expiratory CO₂ level, arterial
246 blood pressure, and lung inflation pressure, on the hard disk of a personal computer via a 16-bit
247 analog-to-digital converter (PowerLab, AD Instruments, 10 kHz sampling rate) and displayed
248 continuously with software (Chart, AD Instruments).

249 ***Electrophysiological recording in situ***

250 To monitor respiratory network activity and motor output in the *in situ* perfused brainstem-spinal
251 cord preparations, we recorded with fire-polished glass suction electrodes inspiratory activity
252 from PN, and cVN inspiratory and post-inspiratory activity. Signals were amplified (50,000 –
253 100,000X, CyberAmp 380, Molecular Devices), band-pass filtered (0.3 – 2 kHz), digitized (10
254 kHz sampling rate) with an AD converter [Cambridge Electronics Design (CED)], and then
255 rectified and integrated digitally with Spike 2 software (CED). Extracellular population activity
256 from pre-BötC or BötC respiratory neurons in the perfused *in situ* preparations was also recorded
257 with a fine glass electrode (3–5 MΩ) filled with 0.5 M Na⁺ acetate.

258 ***Targeting the pre-BötC and BötC regions with microinjections in vivo***

259 To block fast inhibitory transmission a cocktail of GABA_A (gabazine, Sigma) and glycine
260 (strychnine, Sigma) receptor antagonists (in aCSF) was pressure injected (250 μM, 105–115 nl)
261 into the BötC or pre-BötC bilaterally and simultaneously (1–1.5 nl/s) with small diameter
262 (OD = 15 μm, ID = 7.5 μm) polished micropipettes (Drummond Scientific). In another set of
263 experiments the GABA_A agonist muscimol was injected (100 μM, 25–30 nl) into the BötC or
264 pre-BötC bilaterally and simultaneously. Control injections were made at the same sites with
265 aCSF alone. All injection volumes were measured by microscopically observing the change in
266 level of the meniscus within the micropipette. Microinjections were done after

267 electrophysiological recording to map the extracellular single unit/neuronal population activities
268 characteristic of the pre-BötC or BötC regions as described above, and also in some *in vivo*
269 experiments after pharmacological probing by microinjection of 5 nl of 10 mM L-Glutamate (L-
270 Glu) to further confirm locations of the pre-BötC or BötC regions, which have site-specific
271 responses to brief (500 msec) local L-Glu microinjections (i.e., transient apnea with increasing
272 arterial blood pressure (ABP) for the BötC region, and tachypnea with decreasing ABP for the
273 pre-BötC region) (see **Figure 3C,D**). These blood pressure responses are typical because the pre-
274 BötC partially overlaps with the depressor caudal ventrolateral medulla (CVLM) and the BötC
275 with the pressor rostral ventrolateral medulla (RVLM) (Kanjhan et al., 1995; Lipski et al., 1996;
276 Moraes et al., 2012). According to our mapping by extracellular recordings, and consistent with
277 characteristic perturbations obtained by our targeted L-Glu microinjections based on the neuronal
278 activity maps, BötC and pre-BötC in isoflurane anesthetized adult male rats (340–380 g) occupy
279 restricted areas: 1.8–2.1 mm lateral, 550–850 μm depth from the ventral surface and extending
280 ~ 400 μm in the rostro-caudal dimension (i.e., ~ 800 – 1200 μm from the caudal pole of facial
281 nucleus or ~ 1.6 – 2.0 mm rostral to obex) for pre-BötC, and for BötC 1.9–2.2 mm lateral, 450–
282 750 μm depth, and 600–700 μm in the rostro-caudal dimension (~ 100 – 750 μm from the caudal
283 pole of facial nucleus or ~ 2.0 – 2.75 mm rostral to obex). At the end of each experiment
284 fluorescent marker yellow-green microbeads (0.1 μm diameter, 2% solution, Invitrogen) were
285 injected via a pipette (OD = 30 μm , ID = 15 μm , Drummond) into the site of microinjections for
286 *post hoc* morphological verification (**Figures 1 and 2**).

287 Because the locations of pre-BötC and BötC in adult rats relative to the ventral surface
288 are shallow (550–850 and 450–750 μm , respectively), we performed tests for back leakage of
289 injected solution along the microinjection pipette track. Pipettes with different outer diameters

290 (12.5–50 μm) were filled with 2% of pontamine sky blue and only large diameter pipettes (>30
291 μm) showed substantial leak of dye back to the ventral surface during microinjections.
292 Accordingly for drug microinjections *in vivo* we only used pipettes with 15 μm OD that never
293 exhibited back leak.

294 ***Microinjections in arterially perfused brainstem-spinal cord preparations in situ***

295 As *in vivo*, we bilaterally microinjected a cocktail of gabazine and strychnine and in some
296 experiments muscimol (all drugs dissolved in the perfusate aCSF) with micropipettes (ID = 20
297 μm) positioned in the pre-BötC or BötC through the ventral medullary surface with microdrives
298 (Marzhauser) after mapping locations of these regions with extracellular recording of pre-
299 inspiratory (pre-BötC) or expiratory (BötC) neuronal population activities. Slow, continuous
300 microinjection was accomplished by applying low pressure (30 mm Hg) to the pipettes with a
301 pressure control and measurement system. In preliminary experiments we determined that,
302 compared to the *in vivo* experiments, lower concentrations of drugs (30 μM of gabazine and
303 strychnine or 10 μM muscimol) bilaterally injected into either of these regions caused rapid and
304 large disturbances of respiratory motor output and hence all experiments with the perfused
305 brainstem-spinal cord preparations were conducted at these lower drug concentrations. In some
306 experiments, extracellular recordings of neuronal population activity in pre-BötC (during
307 injections in BötC) or BötC (during injections in pre-BötC) regions were made during drug
308 microinjections. Fluorescent microbeads were microinjected to mark the sites of drug
309 microinjection (**Figures 1, 2**) as described above for the *in vivo* experiments.

310 ***Histological verification of microinjection sites***

311 Immediately after marking locations of drug microinjection sites, animals *in vivo* were
312 transcardially perfused with 400 ml of saline (10–12°C, pH 7.4) with heparin (1,000 Units/ml)
313 followed by 500 ml of 4% paraformaldehyde (wt/vol) in 0.1 M phosphate buffered saline (PBS,
314 10–12°C, pH 7.4). A similar procedure was followed (but with smaller volumes of saline and
315 paraformaldehyde perfusates) for perfusion fixation of the *in situ* brainstem-spinal cord
316 preparations. For both preparations the brainstem was removed, post-fixed in the same fixative
317 for 24 h at 4°C, and subsequently cryoprotected by sequential incubation in 15% and 30%
318 sucrose in PBS and stored overnight at 4°C in 30% sucrose, 0.1 M PBS solution. The medulla
319 oblongata was sectioned parasagittally or coronally at 30 or 50 µm thick sections with a freezing
320 microtome. For fluorescence immunohistochemistry, floating sections were incubated with 10%
321 donkey serum in PBS with Triton X-100 (0.3%) and subsequently incubated for 48–72 hours at
322 room temperature with primary antibodies for choline acetyltransferase (ChAT) (goat anti-ChAT,
323 Millipore, 1:200) to label motoneurons. Sections were then rinsed with PBS and incubated for 2
324 hours with secondary antibodies for ChAT (donkey anti-goat-Dylight 488, 1:500). Individual
325 sections were mounted on slides and covered with an anti-fading medium (Fluoro-Gel; Electron
326 Microscopy Sciences). Fluorescent labeling was visualized with a laser-scanning confocal
327 imaging system (Zeiss LSM 510).

328 ***Signal analyses of respiratory parameters***

329 All automated analyses of respiratory parameters from digitized nerve or neuronal population
330 activities were performed with IDL software (Exelis VIS). Inspiratory events were detected from
331 digitally rectified and integrated phrenic nerve signals via a 200 ms window moving average and
332 peak detection algorithm that calculated a threshold-based zero derivative (positive peak) point.
333 Following peak detection, inter-burst interval (IBI; inverse of burst frequency), inspiratory time

334 (T_I) and expiratory time (T_E) were measured. T_I was measured as the original integrated burst
335 width at 20% of the peak height above baseline; T_E was calculated as $IBI - T_I$. Inspiratory
336 amplitude (amp.) was calculated by subtracting the local baseline from the peak value. The
337 endpoint of the parameter quantification was defined when the perturbation during or after
338 microinjections reached its maximum or the signals declined to noise level and the program
339 started missing peak detections (which could appear as a quantum jump in IBI).

340 The time courses of the changes in the above parameters for a given experimental group
341 were variable, which we assume resulted from variability in the times required for drug diffusion
342 to affect a sufficient number of neurons to produce the perturbations. To represent group data, we
343 computed the mean time courses of the parameter values by the following procedures. For each
344 experiment, the time courses of the parameters were extracted by a 30 s window moving median
345 up to the defined endpoint, and the parameter values for each time series were normalized to the
346 computed mean values during the control period (from 120 to 0 s before start of microinjection).
347 Each time course was divided into 100 time points representing 1% increments from the start of
348 microinjection (time 0) to the endpoint. We then computed the group mean time, and also mean
349 values of the normalized parameters, at each of these points, which were plotted and connected
350 by lines to represent the mean time series. The mean endpoint was plotted with its \pm SEM's
351 represented by crossbars (see **Figures 4B-E, 6A-D, 7B-E, 9A-D, 13B-E, and 14D-G**) and the
352 SEM's of the preceding normalized parameter values for the group time series were represented
353 by a gray band. To determine statistical significance, the control values were compared with the
354 endpoint values for each experiment within a group using a two-sided Wilcoxon Signed-Rank
355 Test (significant p-value: <0.05).

356 In addition to quantifying the respiratory parameters indicated above, we analyzed
357 perturbations of amplitudes and durations of individual phases of the respiratory cycle (e.g., post-
358 I activity in cVN recordings *in situ*) from integrated, cycle phase-triggered (peri-event)
359 neurograms aligned at the onset of the inspiratory phase defined by PN activity. Successive
360 cycle-triggered traces were either overlaid, or represented as a colored raster plot to depict
361 temporal profiles of activity intensity before and during/after drug injection periods (see **Figures**
362 **10A,B and 14B**).
363

364 **Results**

365 ***Perturbations of respiratory rhythm and pattern by targeted microinjection of L-***

366 ***Glutamate in the pre-BötC or BötC in vivo***

367 As described in Methods, we microinjected L-Glu in pre-BötC and BötC regions (n = 15, 10
368 mM, 5 nl) to establish characteristic regional excitatory perturbations. These *in vivo* experiments
369 demonstrate that activation of pre-BötC (n = 5) by brief (500 msec) L-Glu microinjections
370 always produced a transient increase of respiratory frequency (from 28.9 ± 4.4 to 44.55 ± 6.1
371 bursts/min, $p < 0.0001$) due to a significant reduction of expiratory phase duration (T_E) (**Figure**
372 **3C**). In contrast, the same L-Glu microinjections into BötC (n = 10) always transiently prolonged
373 the respiratory period (by 5.4 to 21 s range; mean value = 10.1 ± 4.03 s) (**Figure 3D**),
374 documenting site-specificity of the perturbations.

375 ***Perturbations of respiratory rhythm and pattern by microinjection of gabazine and***

376 ***strychnine in the pre-BötC in vivo and in situ***

377 Microinjections of the gabazine-strychnine cocktail were performed after initially identifying the
378 pre-BötC region electrophysiologically by recording pre-I/I neuronal population activity and/or
379 also after microinjected L-Glu (*in vivo*) to identify the pre-BötC region (**Figure 3C**).
380 Perturbations of neural activity with bilateral microinjections of 110 nl of 250 μ M of gabazine
381 and strychnine in the anesthetized adult rat *in vivo* were stereotypical. A representative example
382 is shown in **Figure 4A**. Drug microinjections in pre-BötC produced an increase in the respiratory
383 frequency (f_R), primarily due to shortening of T_E , as well as a decrease of the amplitude of
384 integrated PN activity. The group (n = 6) *in vivo* data are summarized in **Figure 4B-E**, which
385 shows the mean time courses of the developing perturbations of all parameters (normalized to

386 control values) during and after the microinjections. Perturbations developed rapidly, within 10 s
387 following the onset of microinjection in all cases. The respiratory frequency increased to $184.8 \pm$
388 5.6% ($p = 0.03$), T_I decreased to $71.3 \pm 4.5\%$ ($p = 0.03$), and T_E was reduced to $52.6 \pm 3.2\%$ ($p \leq$
389 0.03) of control values. The amplitude of integrated PN activity decreased to $32.1 \pm 3.9\%$ ($p \leq$
390 0.03) of pre-injection control values. These parameter values, all of which are statistically
391 significant, were obtained at 95.83 ± 10.03 s after onset of the microinjections when the
392 perturbations approached maximum values. The average injection time for the group was $57.66 \pm$
393 22.09 s. After these perturbations the time required for recovery of inspiratory activity with a
394 pattern resembling the control activity was variable, but usually a period of minimally 40 min.
395 was required *in vivo*.

396 Similarly rapid and large perturbations were caused by bilateral microinjections of $30 \mu\text{M}$
397 gabazine-strychnine within the pre-BötC of *in situ* perfused juvenile rat brainstem-spinal cord
398 preparations ($n = 6$, **Figure 5A and B**). Figure 5A shows a typical example of the large
399 disturbances of the respiratory frequency and amplitudes of activity recorded from PN and cVN,
400 including the pronounced increase in the frequency of PN inspiratory discharge accompanied by
401 reductions in discharge amplitude. In the example shown in **Figure 5B**, the augmented frequency
402 of PN inspiratory discharge culminated in tonic activity, which occurred in 1/6 experiments. For
403 the group data mean values of respiratory frequency increased to $175.9 \pm 18.0\%$ ($p = 0.03$), T_I
404 slightly increased to $110.4 \pm 4.0\%$ ($p = 0.03$), and T_E decreased to $43.7 \pm 8.0\%$ ($p = 0.03$) of
405 control values (**Figure 6A-C**). The integrated PN activity amplitude decreased to $62.3 \pm 6.0\%$ (p
406 $= 0.03$) (**Figure 6D**). These disturbances followed a similar time course to those *in vivo* and were
407 measured at 84.1 ± 17 s after the onset of microinjections (average injection time of 178.3 s)
408 when maximum changes in parameter values obtained. Recovery of control patterns of nerve

409 activity typically occurred 15-20 min. after terminating the bilateral microinjections in these *in*
410 *situ* experiments.

411 ***Disruption of respiratory rhythm and pattern by microinjection of gabazine and***
412 ***strychnine in the BötC in vivo and in situ***

413 Bilateral microinjections of gabazine-strychnine were performed in the BötC region after
414 identifying this region by extracellular recording of augmenting expiratory and/or post-I
415 neuronal population activity *in situ* and *in vivo*, and in some ($n = 3/6$) of the *in vivo* experiments
416 in this group, after confirming the characteristic suppression of recorded phrenic discharge and
417 pressor blood pressure responses by L-Glu microinjections. In contrast to the results obtained
418 with microinjections in the pre-BötC, bilateral microinjections of 110 nl of 250 μM gabazine and
419 strychnine into the BötC *in vivo* (**Figure 7**, $n = 6$), and also the microinjections in the *in situ*
420 experiments with the lower concentrations of the inhibitory receptor antagonists (**Figures 8 and**
421 **9**, $n = 6$), significantly reduced the frequency of integrated PN discharge due primarily to a
422 prolongation of T_E , accompanied by a reduction of T_I and the amplitude of integrated PN
423 activity. For the averaged group *in vivo* data (**Figure 7B-E**), at 36.66 ± 6.4 s following the onset
424 of microinjections, the respiratory frequency decreased to $25.8 \pm 8.0\%$ ($p \leq 0.03$), T_I was reduced
425 to $88.4 \pm 5.3\%$ ($p \leq 0.06$), and T_E increased to $257.2 \pm 48.0\%$ ($p \leq 0.03$) of control values. The
426 amplitude of integrated phrenic discharge decreased to $39.9 \pm 13.8\%$ ($p \leq 0.03$) of control values
427 (**Figure 7E**). In two *in vivo* experiments, rhythmic inspiratory discharge was completely
428 suppressed for ≥ 20 s (see example in **Figure 7A**). The average microinjection time for the group
429 was 53.67 ± 19.32 s.

430 Similar perturbations occurred with bilateral microinjections of 30 μM gabazine-
431 strychnine in the BötC *in situ* (**Figures 8 and 9**). For the averaged group data ($n = 6$, **Figure 9A-**

432 C) at 92.5 ± 16.77 s after injection onset, inspiratory frequency decreased to $22.6 \pm 10.7\%$ ($p =$
433 0.03), T_E increased to $430.2 \pm 17.3\%$ ($p = 0.03$), and T_I decreased to $56.2 \pm 13.0\%$, ($p = 0.03$) of
434 pre-injection control values. Integrated PN discharge amplitude was reduced to $15.4 \pm 7.0\%$ ($p =$
435 0.03) (**Figure 9D**). In three of these *in situ* experiments, rhythmic inspiratory activity was
436 transiently suppressed for ≥ 20 s (examples shown in **Figure 8**). These perturbations were
437 reflected in simultaneously recorded cVN inspiratory activity (**Figure 8A**) in all experiments
438 analyzed and by recorded pre-BötC pre-I/I population activity (illustrated in **Figure 8B**) in two
439 of these experiments, which demonstrate that the perturbations in BötC disrupt pre-BötC
440 neuronal activity. In all experiments post-inspiratory (post-I) cVN discharge was also disrupted
441 (below) and in one experiment tonic discharge on the cVN was recorded during the disruption of
442 rhythmic motor output (**Figure 8A**). With the bilateral injections of the inhibitory receptor
443 antagonists in the BötC *in situ* or *in vivo*, although nerve activity could emerge after transient
444 suppression of motor output (e.g., Figures 7A and 8A), such activity was disturbed relative to
445 control activity. In all of these experiments, typically 15-25 min. *in situ* and 40-60 min. *in vivo*
446 were required to recover activity resembling control patterns of motoneuronal discharge.

447 ***Disruption of three-phase respiratory pattern by blocking inhibition in the pre-BötC or***
448 ***BötC in situ***

449 The microinjections of gabazine-strychnine in either the pre-BötC ($n = 6$) or BötC ($n = 6$) *in situ*
450 disrupted the three-phase respiratory motor output pattern as analyzed from simultaneous
451 recordings of PN and cVN activity, the latter of which always exhibited prominent post-I
452 discharge. Cycle-triggered averages and time-series raster plots of integrated PN and cVN shown
453 in **Figure 10A,B** illustrate that cVN post-I activity is eliminated as GABA_Aergic and glycinergic
454 inhibition is attenuated in either region. This loss of post-I activity as the drug-induced

455 perturbation develops represents a transformation from a three-phase to a two-phase motor
456 output pattern (Smith et al., 2007).

457 ***Site-specific perturbations of rhythm and pattern by microinjections of muscimol in the***
458 ***pre-BötC and BötC in vivo and in situ***

459 The differential perturbations of inspiratory discharge frequency with the GABA_A and glycine
460 receptor antagonists in the BötC (frequency decrease) vs. the pre-BötC (frequency increase)
461 demonstrate site-specificity of the perturbations. To further test for site specific perturbations by
462 manipulating local inhibition, we regionally inhibited/attenuated neuronal activity by bilateral
463 microinjection of the GABA_A receptor agonist muscimol. In these experiments, the pre-BötC and
464 BötC regions were first identified electrophysiologically by extracellular recording and/or by
465 microinjection of L-Glu *in vivo*. As illustrated in **Figure 11**, bilateral microinjection of 25–30 nl
466 of 100 μM muscimol in the pre-BötC *in vivo* progressively reduced the frequency and amplitude
467 of phrenic discharge and eliminated inspiratory motor output within 20 s in all experiments (n =
468 7). The suppression of inspiratory activity persisted for 40.1 ± 26.8 s during which rhythmic
469 inspiratory activity could be restored immediately by subsequent bilateral microinjection of 110
470 nl of 250 μM gabazine at the same site (**Figure 11**). This latter result also demonstrated the
471 efficacy of gabazine at the concentrations employed in our experiments to antagonize activation
472 of GABA_A receptors in a regionally specific manner. Bilateral microinjections of lower
473 concentrations of muscimol (10 μM) in the pre-BötC in the *in situ* preparations (n = 5) also
474 rapidly suppressed phrenic inspiratory activity (**Figure 12**).

475 In experiments targeting the BötC *in vivo* (n = 7), bilateral microinjection of the same
476 volume and concentration of muscimol progressively increased discharge frequency, due
477 primarily to a reduction of T_E, and reduced the amplitude of integrated phrenic inspiratory

478 discharge (**Figure 13**). For the averaged group *in vivo* data at 486.4 ± 67.6 s after injection onset,
479 integrated phrenic discharge amplitude was reduced to $58.9 \pm 8.9\%$ ($p = 0.015$), inspiratory
480 frequency increased to $175.19 \pm 8.4\%$ ($p = 0.015$), T_E decreased to $51.4 \pm 3.3\%$ ($p = 0.015$), and
481 T_I decreased to $83.4 \pm 3.3\%$ ($p = 0.015$) of pre-injection control values (**Figure 13B-D**).
482 Comparable perturbations were obtained with bilateral microinjections of $10\mu\text{M}$ muscimol in the
483 *in situ* preparations (**Figure 14**, $n = 6$). At 139 ± 20 s following the onset of the microinjections,
484 the group averaged inspiratory frequency increased to $148.1 \pm 16.88\%$ ($p = 0.03$), T_E decreased
485 to $53.1 \pm 8.0\%$ ($p = 0.03$), and T_I was essentially unchanged ($99.0 \pm 15.3\%$ of pre-injection
486 values, $p = 1.0$) (**Figure 14D-F**). The integrated phrenic discharge amplitude was reduced to 75.4
487 $\pm 6.4\%$ ($p = 0.03$) (**Figure 14G**). In addition, integrated cVN post-I activity was progressively
488 reduced and eliminated by muscimol in the BötC *in situ* (**Figure 14B**).
489

490 **Discussion**

491 *Role of synaptic inhibition within and between pre-BötC and BötC for respiratory*

492 *rhythm and pattern generation*

493 For the discussion of the role of synaptic inhibition in respiratory rhythm and pattern generation,
494 it is necessary to clarify our definitions of the terms “rhythm” and “pattern”. We define rhythm
495 as the respiratory cycle period/frequency. Respiratory pattern is defined as all features of activity
496 occurring within the respiratory cycle, including the presence and coordination of the different
497 activity phases (inspiratory, post-inspiratory, late expiratory) as recorded from neuronal
498 populations/nerve motor output activity, as well as the durations, amplitudes, and shapes of
499 integrated activity within phases.

500 Brainstem respiratory networks consist of excitatory and inhibitory circuits distributed
501 within interacting regions of the medulla and pons including the medullary pre-BötC and BötC,
502 which are proposed to contain core circuits involved in respiratory rhythm and pattern
503 generation. While there is general agreement that excitatory pre-BötC circuits generate rhythmic
504 inspiratory activity transmitted to and driving spinal and cranial inspiratory motor outputs,
505 functional roles of inhibitory pre-BötC and BötC circuits continue to be debated (e.g.,
506 Janczewski et al., 2013; Feldman et al., 2013, vs. Smith et al., 2009, 2013; Richter and Smith,
507 2014). It has been postulated that phasic synaptic inhibition originating in these circuits, known
508 to contain populations of rhythmically active glycinergic and GABAergic neurons, are critically
509 involved in generating the three-phase pattern of respiratory neuron activity during normal
510 breathing by shaping firing patterns of active populations of neurons, orchestrating phase
511 transitions, and controlling which populations are inactive during each phase (e.g., Rybak et al.,
512 2004, 2007; Smith et al., 2007, 2009, 2013). Inspiratory and expiratory neurons in these regions

513 receive phasic volleys of inhibitory post-synaptic potentials/currents as clearly established by
514 intracellular recordings (Schmid et al., 1996; Molkov et al., 2012; Shevtsova et al., 2014; Richter
515 and Smith, 2014), and the inhibitory neurons in the pre-BötC and BötC are proposed to interact
516 during the respiratory cycle via mutual inhibitory connections for dynamic control of rhythm
517 generation, although these interactions have not been definitely established experimentally.

518 We have further evaluated roles of the glycinergic and GABAergic synaptic inhibition
519 within the pre-BötC and BötC by regionally disrupting/attenuating this inhibition
520 pharmacologically with specific receptor antagonists, which has been attempted in previous
521 studies in several species (cat, rat, rabbit) *in vivo*, most recently in adult rats with conflicting
522 results (Janczewski et al., 2013). In the present experiments we have established that
523 pharmacologically attenuating GABA_A and glycine receptor-mediated inhibition in the pre-BötC
524 or BötC causes major site-specific perturbations of respiratory rhythm and pattern both in
525 anesthetized, vagotomized adult rats *in vivo* and unanaesthetized, vagotomized juvenile rat
526 perfused brainstem-spinal cord preparations *in situ*. The results obtained *in vivo* and *in situ* are
527 congruent and confirm that:

528 (1) Blocking inhibition in the pre-BötC augmented inspiratory discharge frequency due to
529 a shortening of T_E , reduced inspiratory discharge amplitude, and eliminated post-I activity
530 thereby disrupting the normal three-phase respiratory pattern. In some cases rhythmic motor
531 output was completely terminated.

532 (2) Blocking inhibition in the BötC reduced inspiratory discharge frequency associated
533 with a lengthened T_E , reduced the amplitude of inspiratory discharge, disrupted the three-phase
534 pattern due to a loss of rhythmic post-I activity, and in some cases transiently terminated
535 inspiratory motor output accompanying a loss of pre-BötC inspiratory activity.

536 Therefore, we conclude that ongoing glycinergic and GABA_Aergic inhibition in pre-BötC
537 and BötC circuits are fundamentally involved in dynamical regulation of respiratory rhythm
538 generation and are required for generating the normal three-phase respiratory pattern. Our studies
539 also confirm a fundamental role of BötC inhibitory circuits and their interactions with pre-BötC
540 inspiratory rhythm generating circuits.

541 ***Comparisons with results from previous targeted pharmacology studies***

542 Our results, obtained in juvenile and adult rats, are consistent with previous studies in
543 anesthetized, non-vagotomized adult cats (Pierrefiche et al., 1998) demonstrating that bilateral
544 pharmacological disruption of glycinergic synaptic inhibition with strychnine in the pre-BötC
545 reduces inspiratory discharge amplitude and markedly augments inspiratory discharge frequency
546 or totally abolishes rhythmic phrenic nerve activity. In their studies, simultaneous block of
547 GABA_Aergic and glycinergic inhibition led to sustained tonic discharge on phrenic nerves,
548 indicating disruption of rhythmic inspiratory motor output. Furthermore, results obtained in
549 anesthetized vagotomized adult rabbits by Bongianni et al. (2010) also demonstrated that
550 bilateral block/attenuation of glycinergic inhibition in the pre-BötC augmented inspiratory
551 frequency and reduced inspiratory discharge amplitude. Also, blocking GABAergic inhibition
552 with gabazine in the BötC strongly depressed inspiratory amplitude and frequency leading to
553 apnea as we demonstrated with GABA_Aergic and glycinergic antagonists in several cases.
554 Moreover, in these studies in rabbits, bilateral microinjection of muscimol in the BötC potently
555 augmented inspiratory discharge frequency and caused loss of rhythmic inspiratory activity that
556 was replaced by tonic discharge of phrenic nerves.

557 The general conclusions from these previous studies in both vagotomized and vagus-
558 intact animals, similar to our conclusions, are that ongoing neuronal GABA_A and glycine

559 receptor-mediated postsynaptic inhibition in the pre-BötC and BötC have a major role in
560 controlling the frequency and amplitude of inspiratory circuit activity during eupneic breathing
561 *in vivo*. Other results obtained by pharmacologically blocking glycinergic inhibition with
562 systemically applied strychnine in perfused rat and mouse brainstem-spinal cord preparations *in*
563 *situ*, disturbing synaptic inhibition throughout the respiratory network, also demonstrate major
564 disturbances of respiratory rhythm and disruption of the three-phase respiratory pattern at
565 cellular and circuit levels (e.g., Shevtsova et al. 2011, 2014; Richter and Smith, 2014).

566 All of the above results and conclusions contrast with those from the recent
567 pharmacological study by Janczewski et al. (2013) performed in anesthetized spontaneously
568 breathing, vagus-intact or vagotomized adult rats *in vivo*. They reported that sequential bilateral
569 microinjections of bicuculline and strychnine in the pre-BötC and then BötC via a ventral surface
570 approach does not significantly disturb inspiratory frequency in vagotomized rats, whereas in
571 vagus-intact rats inspiratory frequency was significantly reduced, accompanied by a prolongation
572 of T_I and T_E — perturbations that the authors attributed to only suppression of the Breuer-Hering
573 inspiratory inhibitory reflex (BHIR), supported by their results showing that the HBIR is blocked
574 by antagonizing synaptic inhibition in the pre-BötC. Other results presented suggested that block
575 of inhibition in the pre-BötC and BötC does not disturb generation of laryngeal post-I activity in
576 vagus-intact rats and thus they concluded that inhibitory circuit interactions do not participate in
577 normal three-phase respiratory pattern generation. This result conflicts with our present and
578 previous results (Shevtsova et al., 2011) *in situ*, where we could routinely record post-I activity
579 on cVN or post-I neuronal activity in this unanaesthetized preparation, and found that disruption
580 of synaptic inhibition in the pre-BötC or BötC consistently eliminated post-I activity. Another
581 major result by Janczewski et al. (2013) was that bilateral ablation of the BötC did not

582 significantly perturb inspiratory frequency or inspiratory-expiratory phase durations, from which
583 they concluded that the BötC is not involved at all in generating the three-phase rhythmic
584 respiratory pattern. This clearly contrasts with our results and those of Bongianni et al. (2010)
585 that disrupting inhibition in the BötC can cause apnea, whereas suppressing BötC neuronal
586 activity with muscimol augments inspiratory frequency and can lead to apneustic-like tonic
587 discharge, similar to disrupting inhibition in the pre-BötC. Janczewski et al. (2013) presented
588 data showing a similar augmentation of frequency leading to tonic discharge and disruption of
589 rhythm generation with muscimol injections in the pre-BötC, which is the opposite of ours and
590 previous results that suppressing neuronal activity with muscimol in the pre-BötC potentially
591 reduces inspiratory frequency and rapidly terminates inspiratory rhythm generation. Overall
592 Janczewski et al. (2013) concluded that inhibition is not required for a normal eupneic breathing
593 rhythm *in vivo* except for mediation of the HBIR in vagus-intact animals.

594 These major discrepancies are not readily resolved. The results obtained with these
595 targeted pharmacological approaches depend critically on accurate site-directed delivery of the
596 inhibitory agonists/antagonists, the ability to antagonize inhibitory post-synaptic receptors on a
597 sufficient number of neurons by regional spread of the antagonists/agonists to ultimately perturb
598 motor outputs, and also on regionally confining the pharmacological perturbations. In our
599 experiments, we verified locations of injection sites histologically and we consistently obtained
600 differential, regionally specific perturbations of inspiratory rhythm: slowing of the rhythm in all
601 cases by inhibitory antagonists in BötC, and contrasting augmented inspiratory frequency with
602 antagonists in pre-BötC. Our reconstructed microinjection sites appear to be identical to the sites
603 reconstructed by Janczewski et al. (compare our **Figure 1** with Figure 1 in Janczewski et al.
604 2013). In our *in vivo* experiments employing a similar ventral surface approach in adult

605 anesthetized rats, we used identical concentrations and ejection volumes of antagonists, which
606 we also showed at least for gabazine had pharmacologically effective GABA_A receptor
607 antagonist-agonist interactions (e.g., **Figure 11**). With our targeting procedures, which included
608 mapping of characteristic neuronal activity profiles as well as differential respiratory and blood
609 pressure responses to local L-Glu microinjections, we also consistently obtained regionally
610 specific perturbations with muscimol microinjections at targeted sites: reduced inspiratory
611 frequency and apnea in the pre-BötC, but augmented inspiratory frequency in the BötC. This
612 specificity also suggests that it was possible to confine actions of the agonists/antagonists to the
613 targeted region. Differences in the numbers of neurons and inhibitory synapses affected by local
614 diffusion of the antagonists might contribute, although assuming accuracy of targeting, we would
615 expect similar perturbations since ejection volumes and antagonist concentrations employed *in*
616 *vivo* were identical.

617 ***Relation to studies employing selective targeting of inhibitory neurons***

618 In a recent study employing optogenetic approaches to selectively stimulate or inhibit pre-BötC
619 glycinergic neurons by virally-transduced expression of photosensitive opsins channelrhodopsin
620 (ChR2) or archaerhodopsin in spontaneously breathing adult mice *in vivo*, Sherman et al. (2015)
621 recently found that optical stimulation of this subset of inhibitory neurons in pre-BötC *in vivo*
622 can terminate inspiration, delay the onset of inspiration with photoactivation during the
623 expiratory phase, and produce long-lasting apnea with prolonged photostimulation. Conversely
624 prolonged photoinhibition augmented the amplitude and frequency of inspiratory activity and
625 could reverse reflex-induced apneas. This approach can provide important information on
626 dynamic perturbations resulting from augmentation or loss of inhibitory neuron function (Abdala
627 et al., 2015) and their results demonstrate that at least pre-BötC glycinergic neuron activity can

628 strongly modulate ongoing inspiratory rhythm and pattern generation. The authors concluded,
629 however, that glycinergic inhibition is not essentially involved in rhythmogenesis despite these
630 perturbations since inspiratory rhythm persisted after photoinhibition, although as the authors
631 discuss it is unclear if sufficient numbers of glycinergic neurons were optically silenced to reveal
632 full effects of pre-BötC glycinergic neuron activity on rhythm generation.

633 Another important consideration for interpreting the significance of these results is that
634 silencing pre-BötC glycinergic neurons may not be analogous to pharmacologically blocking
635 even postsynaptic glycinergic receptors, particularly since relevant glycinergic synapses may
636 originate from neurons outside of the pre-BötC such as BötC neurons not transduced in sufficient
637 numbers with viral vectors targeted to the pre-BötC. These optogenetic results also cannot be
638 readily compared with the effects of pharmacological blockade of both glycinergic and
639 GABA_Aergic postsynaptic inhibition. As known, pre-BötC contains inhibitory neurons with each
640 type of transmission, as well as neurons co-expressing both GABA and glycine (Koizumi et al.
641 2013), so all these neuron types would have to be optically inhibited to fully evaluate the
642 functional role of local inhibitory circuits in the pre-BötC. The augmented inspiratory frequency
643 that we observed with disrupting inhibition in the pre-BötC, which has also been observed by
644 pharmacologically attenuating only glycinergic inhibition with strychnine (e.g., Pierrefiche et al.
645 1998) as discussed above, is a common result of both pharmacological and optical approaches.
646 However, inspiratory amplitude was always markedly reduced, not augmented, by
647 pharmacologically perturbing postsynaptic inhibition in the pre-BötC, suggesting that more
648 complex inhibitory interactions in pre-BötC inspiratory rhythm generation circuits are revealed
649 by the pharmacological approaches. Experiments were not presented by Sherman et al. (2015) on
650 photostimulation/inhibition of glycinergic neurons in the BötC. Optical stimulation of BötC

651 neurons transduced with ChR2, although not selectively in GABAergic and glycinergic neurons
652 but likely including these neurons in these studies, strongly suppresses inspiratory activity in
653 contrast to the powerful augmentation of frequency with photostimulation of pre-BötC neurons
654 in anesthetized rats *in vivo* (Alsaifi et al., 2015). These observations are analogous to our
655 results with local glutamate microinjections, which also do not selectively stimulate specific
656 neuronal phenotypes in these regions.

657 ***Normal eupneic rhythm generation in the absence of synaptic inhibition in vivo?***

658 A continuing debate is whether a normal eupneic inspiratory rhythm and respiratory pattern can
659 be generated without synaptic inhibition in the pre-BötC in the intact system where the pre-BötC
660 interacts with the BötC and other sources of phasic/tonic synaptic inhibition. We show that
661 disrupting pre-BötC synaptic inhibition leads to either higher frequency oscillations accompanied
662 by a large reduction in the amplitude of pre-BötC/phrenic inspiratory activity, or to tonic phrenic
663 nerve activity in some cases, indicating that a normal eupneic inspiratory rhythm generally does
664 not occur in the absence of synaptic inhibition. The variable persistence of inspiratory rhythmic
665 activity in other cases, albeit with large disturbances of the inspiratory rhythm and inspiratory-
666 expiratory pattern, indicates that either we did not sufficiently block postsynaptic inhibition in
667 the pre-BötC with our targeted pharmacological approach in these cases, or some form of
668 inspiratory rhythm generation occurs after disruption of GABA_Aergic and glycinergic inhibition
669 in the intact system. The former is a technical problem that is difficult to solve. This would
670 require extensive local intracellular recordings to analyze endogenous postsynaptic inhibitory
671 potentials simultaneously with the pharmacological perturbations. In our approach, we limited
672 the microinjection volumes of the pipette solution containing inhibitory antagonists, in an
673 attempt to achieve site-specificity of the perturbations. This may have precluded sufficient

674 inhibitory receptor block throughout the local circuits to cause complete disruption of inspiratory
675 rhythm generation in these cases. On the other hand, pre-BötC excitatory neurons and circuits
676 have intrinsic rhythmogenic properties (Smith et al., 2007; St. John et al., 2009; Richter and
677 Smith, 2014), so it is possible that some form of inspiratory rhythm generation, albeit abnormal,
678 can persist in the absence of synaptic inhibition in the intact juvenile/adult system, as occurs in
679 the neonatal rat/mouse pre-BötC isolated in slices *in vitro*.

680 Our models of excitatory and inhibitory pre-BötC circuits and their interactions with
681 BötC inhibitory neurons in the intact system incorporate intrinsic rhythmogenic properties in the
682 excitatory pre-BötC population (Rybak et al., 2004, 2007; Smith et al., 2007; Rubin et al., 2009).
683 These models indicate that depending on the initial excitation state of the excitatory kernel
684 neurons, the endpoint after complete block of postsynaptic inhibition can either be tonic activity
685 of pre-BötC neurons at high levels of excitation, or rhythmic activity at lower excitation levels. It
686 is clear that to answer the question of whether any form of inspiratory rhythm generation can
687 occur, intracellular recordings will have to be employed to monitor the level of membrane
688 potential and activity patterns during and after local block of postsynaptic inhibition.

689 ***Disorganization of the three-phase respiratory pattern after disrupting postsynaptic***
690 ***inhibition***

691 The three-phase organization of the respiratory pattern at least *in situ* was disrupted
692 accompanying the large disturbances of inspiratory rhythm by blocking inhibition in the pre-
693 BötC or BötC. This confirms that the normal eupneic breathing pattern with appropriately
694 coordinated spinal and cranial motoneuron activity relies on synaptic inhibition in BötC and pre-
695 BötC circuits. These inhibitory circuits normally operate with pontine and other excitatory inputs
696 (Rybak et al., 2004; Smith et al., 2007; Dutschmann and Dick, 2012). The pontine Kölliker-Fuse

697 nucleus projects heavily to both the pre-BötC and BötC affecting their inhibitory interactions.
698 Specifically, pontine input is required to generate post-I activity (Rybak et al., 2004; Smith et al.,
699 2007; Dutschmann and Dick, 2012) so the observed loss of this activity in part reflects disruption
700 of the balance of excitatory and inhibitory interactions. Recent experiments in a transected
701 perfused rat brainstem preparation have confirmed the critical role of the pons in three phase
702 respiratory pattern generation (Jones and Dutschmann, 2016). Previously it has been
703 demonstrated that blocking glycinergic inhibition systemically causes a shift of post-I neuron
704 activity into the inspiratory phase, due to phasic excitation of post-I neurons that is normally
705 shunted by inspiratory phase inhibition (see Richter and Smith, 2014) and this shift causes
706 abnormal glottal constriction during inspiration (Dutschmann and Paton, 2002). This also implies
707 that the shifted post-I inhibitory neurons would provide abnormally timed inhibition during the
708 inspiratory phase, possibly including to inspiratory neurons in bulbospinal circuits downstream
709 from the BötC and pre-BötC, which could contribute to the large reductions of inspiratory
710 amplitude and attenuation of PN ramping inspiratory discharge observed after disrupting
711 inhibition. The loss of the three-phase pattern is predicted from models (e.g., Rybak et al., 2004,
712 2007; Smith et al., 2007; Shevtsova et al., 2011, 2014) after inhibitory block in the BötC, where
713 post-I inhibitory neuronal activity is presumed generated. Our results that the three-phase pattern
714 is also disrupted after blocking inhibition in the pre-BötC may reflect the known presence of
715 post-I neurons in the pre-BötC (Schwarzacher et al., 1995; Alheid and McCrimmon, 2008), and
716 shows that the pre-BötC also plays a role in three-phase pattern generation, conceivably by either
717 interactions with the BötC and/or by local inhibitory circuit interactions, which need to be
718 delineated.

719

720 ***Role of BötC circuits and synaptic inhibition in respiratory pattern generation***

721 A fundamental role for BötC neurons in respiratory pattern generation has been questioned by
722 Janczewski et al. (2013) as noted above. Their conclusion that this region plays no role is
723 incompatible with the present and previous results showing that augmenting BötC neuron
724 activity (by glutamate microinjections) suppresses pre-BötC inspiratory activity whereas
725 suppressing BötC activity (by muscimol) augments pre-BötC inspiratory rhythm. The BötC is
726 known to contain major populations of active excitatory and inhibitory expiratory post-I and aug-
727 E neurons, and this region is critical for generating post-I activity (Burke et al., 2010).
728 Excitatory BötC neurons are thought to be a major source of expiratory activity in the respiratory
729 network including for generation of post-I premotoneuron activity. BötC glycinergic and
730 GABAergic expiratory interneurons are proposed to provide widely distributed network synaptic
731 inhibition during expiration (Jiang and Lipski, 1990; Tian et al., 1999a,b; Ezure et al., 2003a,b).
732 These postulated inhibitory connections include to pre-BötC excitatory and inhibitory inspiratory
733 neurons to provide phasic synaptic inhibition orchestrating rhythmic alternation between
734 expiratory and inspiratory activity in the network. Mutual inhibitory synaptic interactions
735 between BötC inhibitory (post-I and aug-E) expiratory neurons and inhibitory inspiratory (e.g.,
736 early-I) pre-BötC neurons have been proposed to coordinate generation of the three-phase pattern
737 of neuronal activity during eupneic breathing (Rybak et al., 2004, 2007; Smith et al., 2007;
738 Rubin et al., 2009; Shevstova et al., 2011, 2014; Richter and Smith, 2014). Based on these
739 proposed interactions, augmenting BötC activity or disrupting postsynaptic inhibition within the
740 BötC should suppress rhythmic activity in the pre-BötC, assuming in each case that BötC
741 neurons shift from phasic to tonic activity. Correspondingly, suppressing BötC activity should
742 augment inspiratory discharge frequency and, depending on the level of ongoing pre-BötC

743 excitation, this can lead to tonic inspiratory activity. Both of the above are features of the present
744 experimental results.

745 We note that the projections and postsynaptic targets of BötC and pre-BötC inhibitory
746 interneurons, particularly mutual inhibitory connections between these neurons, have not been
747 mapped structurally. Establishing these connections remains an important problem. Nevertheless,
748 our results are consistent with mutual interactions and a fundamental role of the BötC and its
749 expiratory inhibitory neurons in three-phase respiratory pattern generation and control of
750 inspiratory rhythm.

751

752 **References**

- 753 Abdala AP, Paton JFR, Smith JC (2015) Defining inhibitory neurone function in respiratory
754 circuits: opportunities with optogenetics? *J Physiol* 593:3033-3046.
- 755 Alheid GF, McCrimmon DR (2008) The chemical neuroanatomy of breathing. *Respir Physiol*
756 *Neurobiol* 164:3-11.
- 757 Alshafi Z, Dickson CT, Pagliardini S (2015) Optogenetic excitation of preBötzinger complex
758 neurons potently drives inspiratory activity in vivo. *J Physiol* 593:3673-3692.
- 759 Baekey DM, Molkov YI, Paton JFR, Rybak IA, Dick TE (2010) Effect of baroreceptor
760 stimulation on the respiratory pattern: Insights into respiratory-sympathetic interactions.
761 *Respir Physiol & Neurobiol* 174: 135-145.
- 762 Bongianni F, Mutolo D, Cinelli E, Pantaleo T (2010) Respiratory responses induced by
763 blockades of GABA and glycine receptors within the Bötzing complex and the pre-
764 Bötzing complex of the rabbit. *Brain Res* 1344:134-147.
- 765 Burke PGR, Abbott SBG, McMullan S, Goodchild AK, Pilowsky PM (2010) Somatostatin
766 selectively ablates post-inspiratory activity after injection into the Bötzing complex.
767 *Neuroscience* 167: 528-539.
- 768 Dutschmann M, Dick TE (2012) Pontine mechanisms of respiratory control. *Compr Physiol*.
769 2:2443-2469.
- 770 Dutschmann, M, Paton, JF (2002) Glycinergic inhibition is essential for co-ordinating cranial
771 and spinal respiratory motor outputs in the neonatal rat. *J Physiol* 543: 643-653.
- 772 Ezure K, Tanaka I, Kondo M (2003a) Glycine is used as a transmitter by decrementing
773 expiratory neurons of the ventrolateral medulla in the rat. *J Neurosci* 23:8941-8948.

- 774 Ezure K, Tanaka I, Saito Y (2003b) Brainstem and spinal projections of augmenting expiratory
775 neurons in the rat. *Neurosci Res* 45:41-51.
- 776 Feldman JL, Del Negro CA, Gray PA (2013) Understanding the rhythm of breathing: so near, yet
777 so far. *Ann Rev Physiol* 75:423-452.
- 778 Grillner S (2006) Biological pattern generation: the cellular and computational logic of networks
779 in motion. *Neuron* 52:751-766.
- 780 Grundy EM, Chakrabarti MK, Whitwam JG (1986) Efferent phrenic nerve activity during
781 induced changes in arterial pressure. *Br J Anaesth* 58:1414-1421.
- 782 Janczewski WA, Tashima A, Hsu P, Cui Y, Feldman, JL (2013) Role of inhibition in respiratory
783 pattern generation. *J Neurosci* 33:5454-5465.
- 784 Johnson SM, Koshiya N, Smith JC (2001) Isolation of the kernel for respiratory rhythm
785 generation in a novel preparation: the pre-Bötzinger complex “island.” *J Neurophysiol*
786 85:1772-1776.
- 787 Jiang C, Lipski J (1990) Extensive monosynaptic inhibition of ventral respiratory group neurons
788 by augmenting neurons in the Bötzing complex in the cat. *Exp Brain Res* 81:639-648.
- 789 Jones SE, Dutschmann M (2016) Testing the hypothesis of neurodegeneracy in respiratory
790 network function with a priori transected arterially perfused brainstem preparation of rat.
791 *J Neurophysiol* doi: 10.1152/jn.01073.2015 [Epub ahead of print].
- 792 Hopp FA, Seagard JL. (1998) Respiratory responses to selective blockade of carotid sinus
793 baroreceptors in the dog. *Am. J. Physiol.* 275 (Regulatory Integrative Comp. Physiol. 44):
794 R10-R18.

- 795 Kanjhan R, Lipski J, Kruszevska B, Rong WA (1995) Comparative study of pre-sympathetic and
796 Bötzing neurons in the rostral ventrolateral medulla (RVLM) of the rat. *Brain Res*
797 699:19-32.
- 798 Koizumi H, Koshiya N, Chia JX, Cao F, Nugent J, Zhang R, Smith JC (2013) Structural-
799 functional properties of identified excitatory and inhibitory interneurons within pre-
800 Bötzing complex respiratory microcircuits. *J Neurosci* 33:2994-3009.
- 801 Koshiya N, Smith JC (1999) Neuronal pacemaker for breathing visualized in vitro. *Nature* 400:
802 360-363.
- 803 Kuwana S-I, Tsunekawa N, Yanagawa Y, Okada Y, Kuribayashi J, Obata K (2006)
804 Electrophysiological and morphological characteristics of GABAergic respiratory
805 neurons in the mouse pre-Bötzing complex. *Eur J Neurosci* 23:667-674.
- 806 Lindsey BG, Rybak IA, Smith JC (2012) Computational models and emergent properties of
807 respiratory neural networks. *Compr Physiol* 2:1619-1670.
- 808 Lipski J, Kanjhan R, , Kruszevska B, Rong WA, Smith M (1996) Pre-sympathetic neurones in
809 the rostral ventrolateral medulla of the rat: electrophysiology, morphology and
810 relationship to adjacent neuronal groups. *Acta Neurobiol Experiment* 56:373-384.
- 811 Molkov YI, Borgmann A, Zhang R, Rybak IA, Smith JC (2012) Analysis of excitatory and
812 inhibitory interactions at high temporal resolution in core circuits of the respiratory CPG.
813 *BMC Neurosci* 13 (Suppl 1): 39.
- 814 Moraes DJ, Zoccal DB, Machado BH (2012) Sympathoexcitation during chemoreflex active
815 expiration is mediated by L-glutamate in the RVLM/Bötzing complex of rats. *J*
816 *Neurophysiol* 108: 610-623.

- 817 Morgado-Valle C, Baca SM, Feldman JL (2010) Glycinergic pacemaker neurons in preBötzinger
818 complex of neonatal mouse. *J. Neurosci* 30: 3634-3639.
- 819 Paton JFR (1996) A working heart-brainstem preparation of the mouse. *J Neurosci Methods*
820 65:63-68.
- 821 Paton JF, Abdala AP, Koizumi H, Smith JC St-John WM (2006) Respiratory rhythm generation
822 during gasping depends on persistent sodium current. *Nat Neurosci* 9:311-313.
- 823 Pierrefiche O, Schwarzacher SW, Bischoff AM, Richter DW (1998) Blockade of synaptic
824 inhibition within the pre-Bötzinger complex in the cat suppresses respiratory rhythm
825 generation in vivo. *J Physiol* 509: 245-254.
- 826 Richter DW (1996) Neural regulation of respiration: rhythmogenesis and afferent control. In:
827 *Comprehensive Human Physiology: From Cellular Mechanism to Integration*, edited by
828 Gregore R, Windhorts U. Berlin: Springer Verlag, pp. 2079-2095.
- 829 Richter DW, Sellar H. (1975) Baroreceptor effects on medullary respiratory neurones of the cat.
830 *Brain Res* 86:168-171.
- 831 Richter DW, Smith JC (2014) Respiratory rhythm generation in vivo. *Physiology* 29: 58-71.
- 832 Rubin JE, Shevtsova NA, Ermentrout GB, Smith JC, Rybak IA (2009) Multiple rhythmic states
833 in a model of the respiratory central pattern generator. *J Neurophysiol* 101:2146-2165.
- 834 Rybak IA, Abdala AP, Markin SN, Paton JFR, Smith JC (2007) Spatial organization and state-
835 dependent mechanisms for respiratory rhythm and pattern generation. *Prog Brain Res*
836 165:201-220.
- 837 Rybak IA, Shevtsova NA, Paton JF, Dick TE, St-John WM, Morschel M., Dutschmann
838 M. (2004) Modeling the ponto-medullary respiratory network. *Respir Physiol Neurobiol*
839 143:307-319.

- 840 Schmid K, Foutz AS, Denavit-Saubie M (1996) Inhibitions mediated by glycine and GABAA
841 receptors shape the discharge pattern of bulbar respiratory neurons *Brain Res* 710:150-
842 160.
- 843 Schreihofer AM, Stronetta RL, Guyenet PG (1999) Evidence for glycinergic respiratory neurons:
844 Botzinger neurons express mRNA for glycinergic transporter 2. *J Comp Neurol* 407:583-
845 597.
- 846 Schwarzacher SW, Smith JC, Richter DW (1995) Pre-Bötzinger complex in the cat. *J*
847 *Neurophysiol* 73:1452-1461.
- 848 Sherman D, Worrell, Cui Y, Feldman JL (2015) Optogenetic perturbation of preBötzinger
849 complex inhibitory neurons modulates respiratory pattern. *Nat Neurosci* 18: 408-414
- 850 Shevtsova NA, Büsselberg D, Molkov YI, Bischoff AM, Smith JC, Richter DW, Rybak IA (2014)
851 Effects of glycinergic inhibition failure on respiratory rhythm and pattern generation.
852 *Prog Brain Res* 209:25-38.
- 853 Shevtsova NA, Manzke T, Molkov YI, Bischoff A, Smith JC, Rybak IA, Richter DW (2011)
854 Computational modelling of 5-HT receptor-mediated reorganization of the brainstem
855 respiratory network. *Eur J Neurosci* 34:1276-1291.
- 856 Smith JC, Abdala AP, Borgmann A, Rybak IA, Paton JF (2013) Brainstem respiratory networks:
857 building blocks and microcircuits. *Trends Neurosci* 36:152-162.
- 858 Smith JC, Abdala AP, Koizumi H, Rybak IA, Paton JF (2007) Spatial and functional architecture
859 of the mammalian brain stem respiratory network: a hierarchy of three oscillatory
860 mechanisms. *J Neurophysiol* 98:3370-3387.

- 861 Smith JC, Abdala AP, Rybak IA, Paton JF. (2009) Structural and functional architecture of
862 respiratory networks in the mammalian brainstem. *Philos Trans R Soc Lond B Biol Sci*
863 364:2577-2587.
- 864 Smith JC, Ellenberger HH, Ballanyi K, Richter DW, Feldman JL (1991) Pre-Bötzinger complex:
865 a brainstem region that may generate respiratory rhythm in mammals. *Science* 254:726-
866 729.
- 867
- 868 St. John WM, Stornetta RL, Guyenet PG, Paton JF (2009) Location and properties of respiratory
869 neurons with putative intrinsic bursting properties in the rat in situ. *J Physiol* 587:3175-
870 3188.
- 871 Tian, GF, Peever JH, Duffin J (1999a) Bötzing complex, bulbospinal expiratory neurons
872 monosynaptically inhibit ventral respiratory group neurons in the decerebrate rat. *Exp*
873 *Brain Res* 124: 173-180
- 874 Tian GF, Peever JH, Duffin J (1999b) Mutual inhibition between Bötzing-complex bulbospinal
875 expiratory neurons detected with cross-correlation in the decerebrate rat. *Exp Brain Res*
876 125:440-446.
- 877 Virkkia A, Polod O, Gyllenberg M, Aittokallio T (2007) Can carotid body perfusion act as a
878 respiratory controller? *J Theor Biol* 249: 737-748.
- 879 Winter S, Fresemann J, Schnell C, Oku Y, Hirrlinger J, Hulsmann S (2009) Glycinergic
880 interneurons are functionally integrated into the inspiratory network of mouse medullary
881 slices. *Pflugers Arch* 458:59-469.
- 882
- 883

884 **Figure Legends**

885 **Figure 1.** Ventral view of the adult rat medulla and histology illustrating targeted sites for
886 pharmacology experiments *in vivo*. **A**, photograph of adult rat brainstem ventral surface as
887 exposed in the *in vivo* experimental preparations with an overview of targeted locations (caudal
888 to facial motor nucleus, VII) of BötC and pre-BötC as routinely identified by
889 electrophysiological mapping of neuronal activity profiles in the present experiments. **B**,
890 photomicrograph of ventral medullary surface and bilaterally arranged pipettes (blue dye-filled
891 for visualization) as typically configured for near perpendicular penetrations of the ventral
892 surface for simultaneous microinjections. **C**, **D**, confocal microscopic images of parasagittal
893 histological sections (50 μm thick) showing, respectively, examples of targeted sites for
894 microinjection of inhibitory antagonists in the pre-BötC ventral to the semi-compact subdivision
895 of nucleus ambiguus (NA_{sc}), and in the BötC ventral to the compact subdivision of nucleus
896 ambiguus (NA_c). Targeted sites are marked by microinjected solution of fluorescent
897 microspheres (green). NA and VII motoneurons are immuno-labeled by ChAT antibody (red).
898 Rostro-caudal spatial extent of the pre-BötC and BotC compartments are indicated. Other
899 abbreviations: vs– ventral surface.

900

901 **Figure 2.** Confocal microscopic images of histological sections illustrating *post-hoc* validation
902 of microinjection sites marked by fluorescent microspheres (green) in the pre-BötC or BötC
903 regions in fixed sections from anesthetized adult rat *in vivo* preparations and juvenile rat *in situ*
904 brainstem-spinal cord preparations. **A**, **B**, coronal sections (30 μm thick) of fixed tissue at the
905 level of pre-BötC (**A**) and BötC (**B**) from *in vivo* preparations. **C**, **D**, coronal sections (30 μm) of
906 fixed tissue at pre-BötC (**C**) and BötC (**D**) levels from juvenile rat *in situ* brainstem-spinal cord
907 preparations. Subdivisions of nucleus ambiguus (NA_c, compact subdivision, and NA_{sc}, semi-
908 compact subdivision), labeled with ChAT antibody (red), provide regional landmarks for pre-

909 BötC (ventral to NAsc) and BötC (ventral to NAc) levels of the medulla. Each image is taken
910 from serial coronal histological sections obtained from experiments targeting these regions.
911 Labeling with microinjected solution of fluorescent microbeads, with varying extent of local
912 spread, indicates the approximate center of the drug microinjection sites in these examples. Other
913 abbreviations: vs– ventral surface.

914

915 **Figure 3.** Characteristic profiles of extracellularly recorded neuronal population activity and
916 examples of perturbations of inspiratory motor output activity and blood pressure produced by
917 pharmacological excitation of neurons within the pre-BötC or BötC regions in the adult rat *in*
918 *vivo*. **A**, a typical example of pre-inspiratory/inspiratory (pre-I/I) population activity used for the
919 identification of pre-BötC. **B**, an example of post-inspiratory (post-I) and augmenting expiratory
920 (aug-E) population activity (post-I/aug-E, simultaneously recorded in this example) used for the
921 identification of BötC. In both **A** and **B**, the raw recording from the phrenic nerve (PN) and PN
922 integrated activity (\int PN) are shown at the bottom. **C**, a 500 msec duration microinjection of L-
923 Glutamate (Glutamate) in the pre-BötC produced an increase in the \int PN burst frequency (see the
924 trace for integrated PN activity, \int PN), and a transient decrease in the arterial blood pressure
925 (ABP). The respiratory frequency (f_R , bottom trace, green) increased primarily due to reduction
926 in expiratory phase duration (T_E trace, blue) at a relatively unchanged inspiratory duration (T_I
927 trace, red). **D**, a microinjection of L-Glutamate in the BötC caused a rapid suppression of PN
928 activity (see traces for \int PN and inspiratory, T_I , and expiratory, T_E , durations) accompanied by an
929 increase of ABP. In **C** and **D**, L-Glutamate (10 mM, 5 nl) was microinjected bilaterally during
930 the brief (500 msec) pulse; the moments of injections are indicated by brown arrows. Traces for
931 T_I , T_E , and f_R , represent corresponding running time intervals of these parameters before, during,
932 and recovery from L-Glutamate microinjection.

933

934 **Figure 4.** Perturbations of respiratory activity by pharmacologically disrupting GABA_Aergic and
935 glycinergic inhibition in the pre-BötC of anesthetized adult rat *in vivo*. **A**, simultaneous bilateral
936 microinjections of gabazine and strychnine (both 250 μ M delivered by slow microinjections of
937 110 nl during the time interval indicated by the brown bar at the top and blue rectangle) caused
938 an increase of respiratory frequency and a reduction in the integrated phrenic nerve activity
939 amplitude (see JPN trace, top, black). The increase of respiratory frequency (f_R , green trace at the
940 bottom) was mainly due to reductions of expiratory phase duration (T_E , blue trace) accompanied
941 by only a small increase of inspiratory phase duration (T_I , red trace). **B-E**, group mean time
942 series showing developing changes of normalized T_I (panel **B**, red curve), T_E (panel **C**, blue
943 curve), respiratory frequency, f_R (panel **D**, green curve), and JPN amplitude (amp., panel **E**,
944 magenta curve) computed over the time window shown from the start (time = 0) of
945 microinjection. Data were computed from JPN for this representative experimental group (n = 6).
946 Solid colored curves are group mean time and mean normalized parameter values; gray shaded
947 bands are ± 1 SEM for the mean parameter values. Endpoints shown are mean time and
948 normalized parameter values ± 1 SEM for both at the maximal perturbation for the injection
949 periods employed.

950

951 **Figure 5.** Perturbations of respiratory activity by pharmacologically disrupting GABA_Aergic and
952 glycinergic inhibition in the pre-BötC of juvenile rat perfused brainstem-spinal cord *in situ*. **A**,
953 example of experimental recordings illustrating perturbations of integrated PN (JPN) and cVN
954 (jcVN) activities by simultaneous bilateral microinjections of gabazine and strychnine (both 30
955 μ M; injection period indicated by the brown bar at the top and blue rectangle), which caused an
956 increase of respiratory frequency (f_R) due to a reduction in T_E (blue) without significant changes
957 in T_I , and a reduction in amplitude of JPN and jcVN. **B**, example of perturbations where the JPN

958 activity progressed to tonic activity, as indicated by the upward shift of the JPN signal baseline.
959 Analysis of respiratory parameters in this case was performed up to the time point indicated by
960 the vertical dot-dashed line. The progressive reduction in JcVN amplitude in both examples
961 reflects in part a reduction and eventual loss of post-I activity (see **Figure 10** for more detailed
962 analysis).

963

964 **Figure 6.** Group data summarizing changes of respiratory activity parameters by
965 pharmacologically disrupting GABA_Aergic and glycinergic inhibition in the pre-BötC of juvenile
966 rat perfused brainstem-spinal cord *in situ*. **A-D**, mean time series from the start of microinjection
967 showing developing changes of normalized T_I (**A**, red curve), T_E (**B**, blue curve), respiratory
968 frequency, f_R (**C**, green curve), and integrated PN discharge amplitude (**D**, amp., magenta curve),
969 which were computed from JPN for a representative experimental group (n = 6). Solid colored
970 curves are group mean time and normalized parameter values; gray bands are ± 1 SEM for the
971 mean normalized parameter values as in **Figure 4B-E**.

972

973 **Figure 7.** Perturbations of respiratory activity by pharmacologically disrupting of GABA_Aergic
974 and glycinergic inhibition in the BötC of adult rat *in vivo*. **A**, gabazine and strychnine cocktail
975 (110 nl, 250 μM) slowly injected during time period indicated (by the brown bar at the top and
976 blue rectangle), progressively reduced respiratory frequency leading to transient apnea in this
977 example (see JPN trace, top, black). Changes in the inspiratory (T_I, red) and expiratory (T_E, blue)
978 phase durations and respiratory frequency (f_R) are shown at the bottom; f_R was reduced mainly
979 due to prolongation of T_E. **B-E**, mean time series from the start of microinjection showing
980 developing changes of normalized T_I (**B**, red curve), T_E (**C**, blue curve), respiratory frequency, f_R
981 (**D**, green curve), and integrated PN activity amplitude (**E**, magenta curve) for a representative

982 experimental group ($n = 6$). Solid colored curves are group mean time and normalized parameter
983 values; gray bands are ± 1 SEM for the mean normalized parameter values.

984

985 **Figure 8.** Disruption of rhythmic respiratory activity by block/attenuation of GABA_Aergic and
986 glycinergic inhibition in the BötC of *in situ* perfused brainstem-spinal cord preparations.
987 **A and B**, two examples from experiments using different preparations illustrating perturbations
988 caused by microinjections of gabazine and strychnine (30 μ M slowly injected during the period
989 indicated by the brown bars at the top and blue rectangles). As in *the vivo* experiments,
990 respiratory frequency was reduced by a prolonged T_E , integrated phrenic nerve discharge
991 amplitude (JPN) was also reduced, and ultimately apnea occurred. Simultaneously recorded
992 integrated cVN (jcVN) in **A** shows disruption of rhythmic activity and tonic discharge (shift of
993 integrated activity baseline) during apneic period. In **B**, simultaneously recorded integrated pre-
994 BötC pre-I/I population activity from another experiment also reflects the reduction of
995 inspiratory frequency and termination of rhythmic activity during bilateral microinjections of the
996 inhibitory receptor blockers in BötC.

997

998 **Figure 9.** Group data ($n = 6$) summarizing perturbations of respiratory rhythm and motor output
999 pattern parameters by disrupting GABA_Aergic and glycinergic inhibition in the BötC of *in situ*
1000 perfused brainstem-spinal cord preparations. Solid colored curves in these time series are mean
1001 time and normalized parameter values and gray bands are ± 1 SEM for the normalized values of
1002 T_I (**A**), T_E (**B**), respiratory frequency (f_R , **C**), and integrated inspiratory activity amplitude (**D**)
1003 computed from the start of microinjections from recordings of integrated PN activity.

1004

1005 **Figure 10.** Disturbances of three-phase respiratory pattern including disruption of post-
1006 inspiratory (post-I) activity by bilaterally microinjected gabazine and strychnine (30 μ M each) in
1007 the pre-BötC (**A**) or BötC (**B**) of *in situ* perfused juvenile rat brainstem-spinal cord preparations.
1008 Upper traces in **A** and **B** show seven consecutive overlaid and aligned integrated PN (red traces)
1009 and cVN (blue traces) activity signals in the pre-microinjection control period (light red and light
1010 blue larger amplitude traces, respectively) and also seven overlaid traces of recorded signals
1011 during microinjections (dark red and dark blue traces with reduced amplitudes). Simultaneously
1012 recorded pre-BötC pre-I/I population activity before and during microinjections (light and dark
1013 green traces, respectively) is also shown at the top in **B** to indicate activity perturbations in this
1014 region occurring with disruption of inhibition in BötC. Signals are aligned (cycle-triggered) at
1015 the onset of PN inspiratory activity indicated by the vertical dotted line in **A** and **B**. Raster plots
1016 below overlaid traces show consecutive series of inspiratory-onset aligned respiratory cycles
1017 with integrated PN inspiratory (red) and cVN including post-I (blue) activities before and during
1018 microinjections. Arrows on the raster plots indicate time interval over which the overlaid traces
1019 above the raster plots were obtained for the pre-microinjection period. During microinjections in
1020 the pre-BötC or BötC, the amplitude of inspiratory and post-I activity is progressively reduced,
1021 and post-I discharge is eliminated as seen on the aligned (darker) \int cVN traces above the raster
1022 plots and in the raster plots with loss of post-I discharge indicated (white arrow).

1023

1024 **Figure 11.** Suppression of rhythmic inspiratory activity by bilateral microinjection of muscimol
1025 in the pre-BötC of adult rat *in vivo* and gabazine antagonism of GABA_A receptor activation.
1026 Muscimol (30 nl, 100 μ M) microinjection (during yellow shaded area) rapidly reduced integrated
1027 PN activity and produced a long-lasting suppression of inspiratory activity that could be restored
1028 by bilateral microinjection of gabazine (110 nl, 250 μ M) at the same site in the pre-BötC (blue
1029 shaded area). Abbreviations (\int PN, T_E, T_I, f_R) are the same as for previous figures.

1030

1031 **Figure 12.** Illustration of prolonged suppression of rhythmic inspiratory activity by bilateral
1032 microinjection of muscimol (10 μ M) in the pre-BötC (yellow shaded area) of juvenile rat
1033 perfused brainstem-spinal cord *in situ*. As *in vivo*, muscimol rapidly reduces PN inspiratory
1034 discharge frequency and terminates inspiratory activity. Abbreviations (JPN , T_E , T_I , f_R) are the
1035 same as for previous figures.

1036

1037 **Figure 13.** Perturbation of inspiratory activity by bilateral microinjection of muscimol in the
1038 BötC of anesthetized adult rat *in vivo*. **A**, muscimol (30 nl, 100 μ M) slowly microinjected
1039 (brown bar at the top and yellow rectangle) in the BötC augments PN frequency due to a
1040 reduction of T_E . **B-E**, mean time series for group data ($n = 7$) summarizing perturbations of
1041 respiratory rhythm and motor output pattern parameters. Solid colored curves are mean time and
1042 normalized parameter values and gray bands are ± 1 SEM of T_I (**B**), T_E (**C**), respiratory
1043 frequency (f_R , **D**), and integrated inspiratory activity amplitude (**E**) computed from recordings of
1044 integrated phrenic nerve activity as in previous figures.

1045

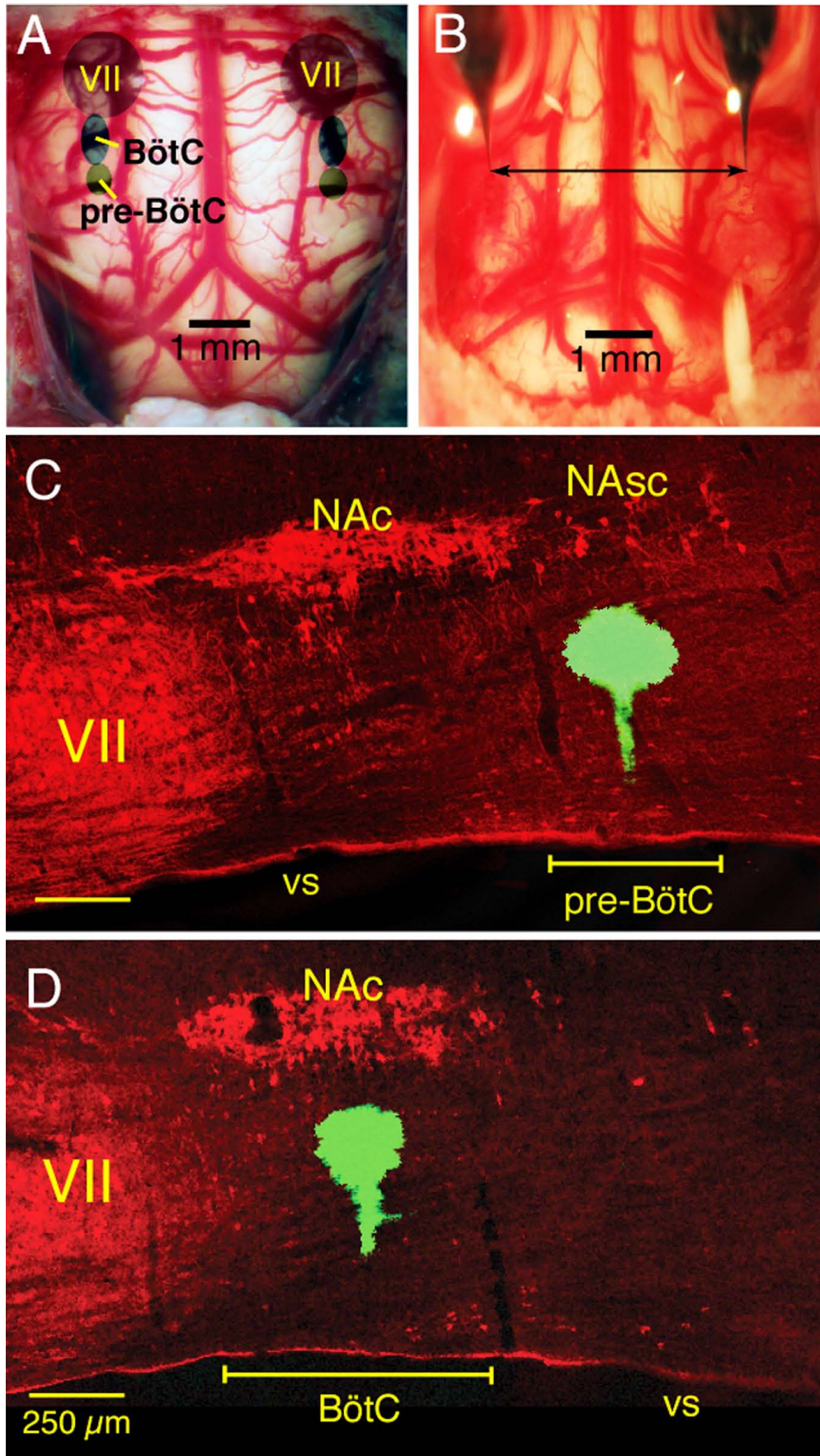
1046 **Figure 14.** Disturbances of respiratory pattern including elimination of post-inspiratory activity
1047 by bilateral microinjection of muscimol (10 μ M) in the BötC of juvenile rat perfused brainstem-
1048 spinal cord *in situ*. **A**, representative example of augmented JPN inspiratory discharge frequency
1049 and pronounced reduction of cVN integrated ($JcVN$) activity amplitude due to suppression of
1050 post-I activity. Overlaid traces in **B** and time series raster plot in **C** of consecutive respiratory
1051 cycles aligned to inspiratory onset (indicated by vertical dotted line in **B**) illustrate perturbations
1052 of cVN post-I discharge during BötC muscimol microinjection in another experiment. In **B**,
1053 integrated PN (red traces) and cVN (blue traces) activity are shown before (lighter red and
1054 lighter blue traces, respectively) and after (dark red and dark blue traces) muscimol
1055 microinjection. Aligned traces of JPN (red) and $JcVN$ (blue) are shown in raster plot in **C** with
1056 the loss of post-I cVN discharge indicated (white arrow), which is also clearly seen from the
1057 $JcVN$ traces (dark blue) above. **D-G**, mean time series for group data ($n = 6$) summarizing
1058 perturbations of respiratory rhythm/pattern parameters. Solid colored curves are mean time and

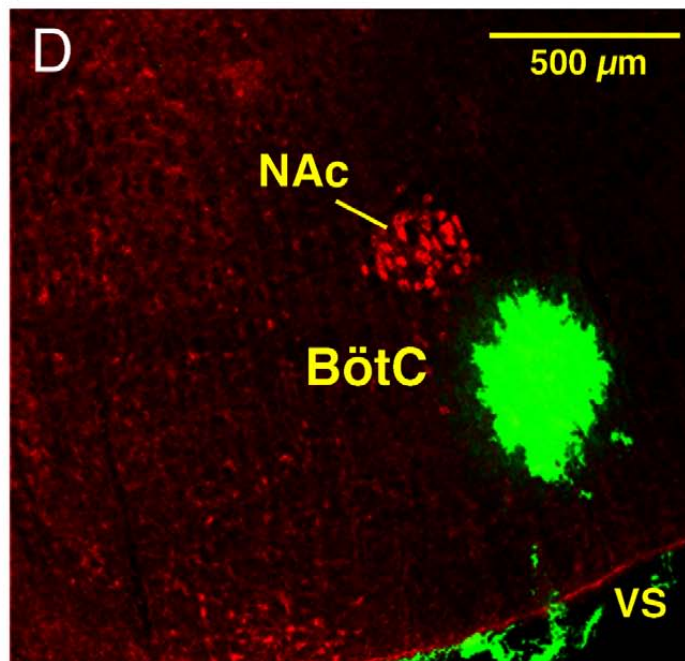
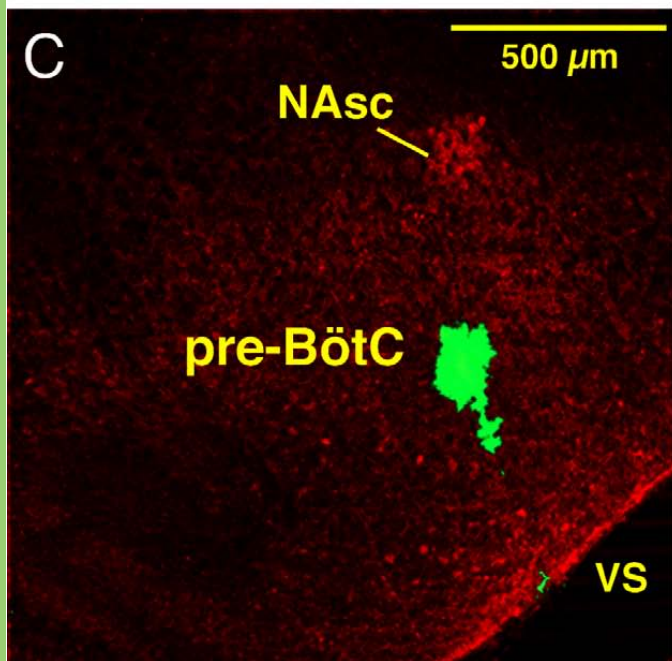
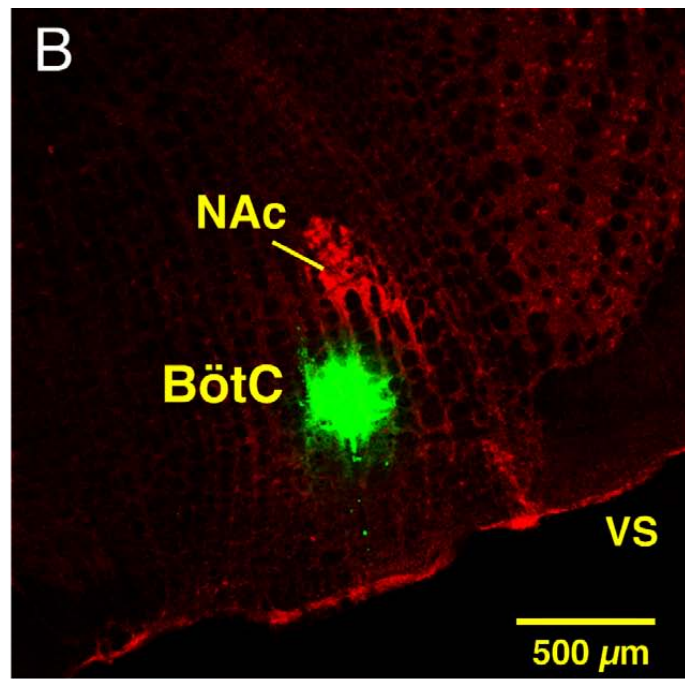
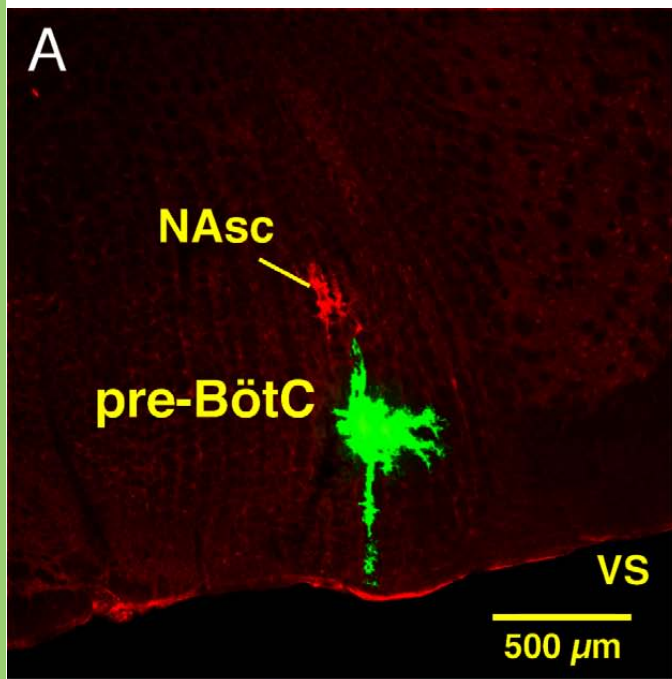
1059 parameter values and gray bands are ± 1 SEM of normalized T_I (**D**), T_E (**E**), inspiratory
1060 frequency (f_R) (**F**), and integrated inspiratory activity amplitude (**G**) computed from recordings
1061 of integrated PN activity.

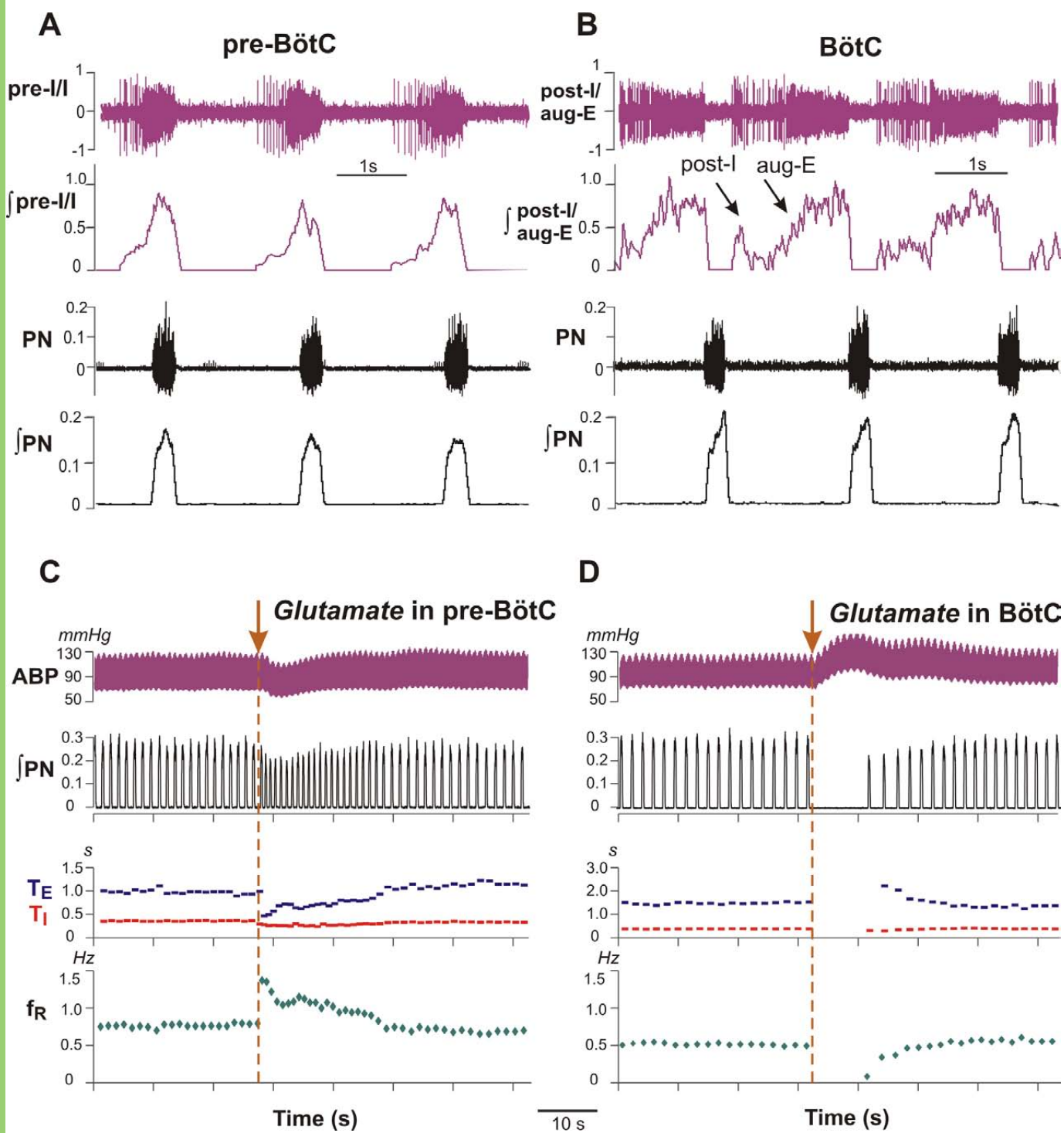
1062

1063

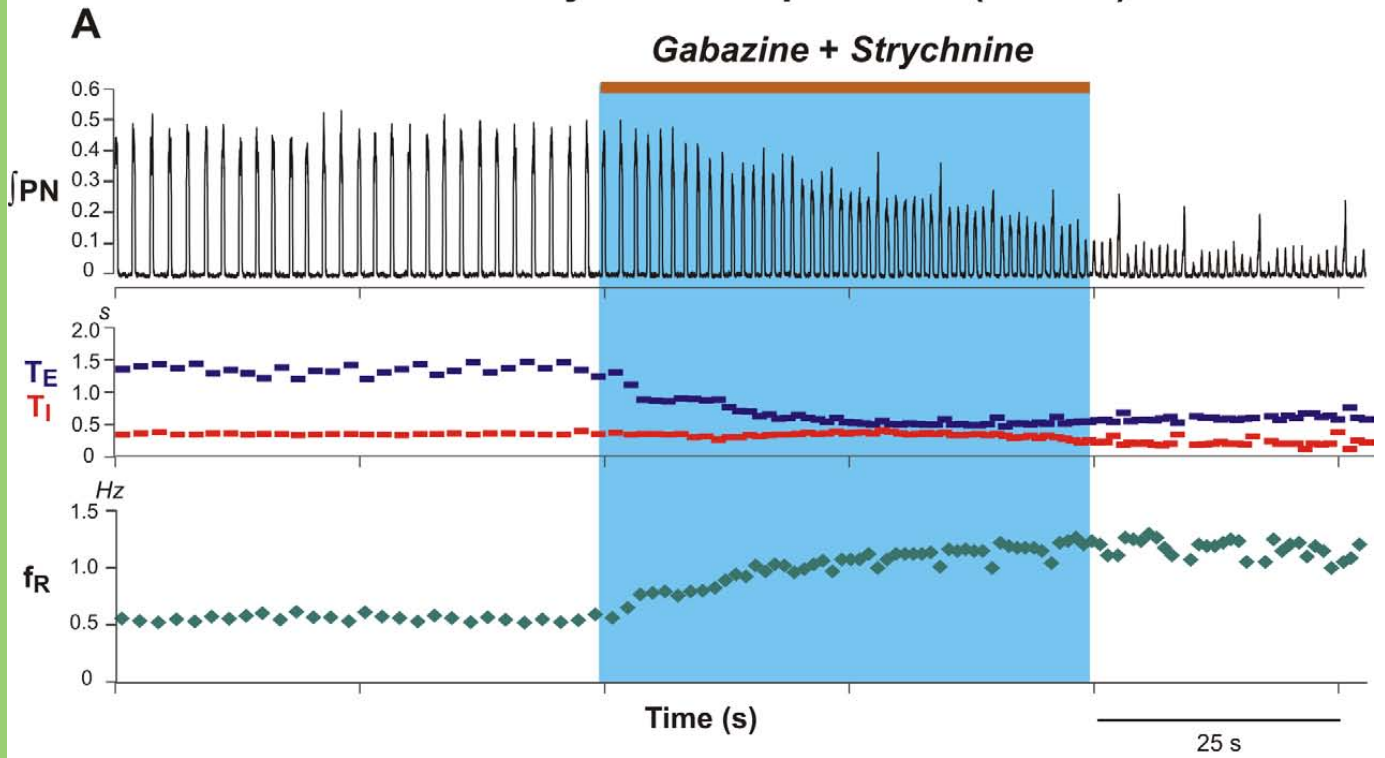
1064 **Visual Abstract.** See abstract



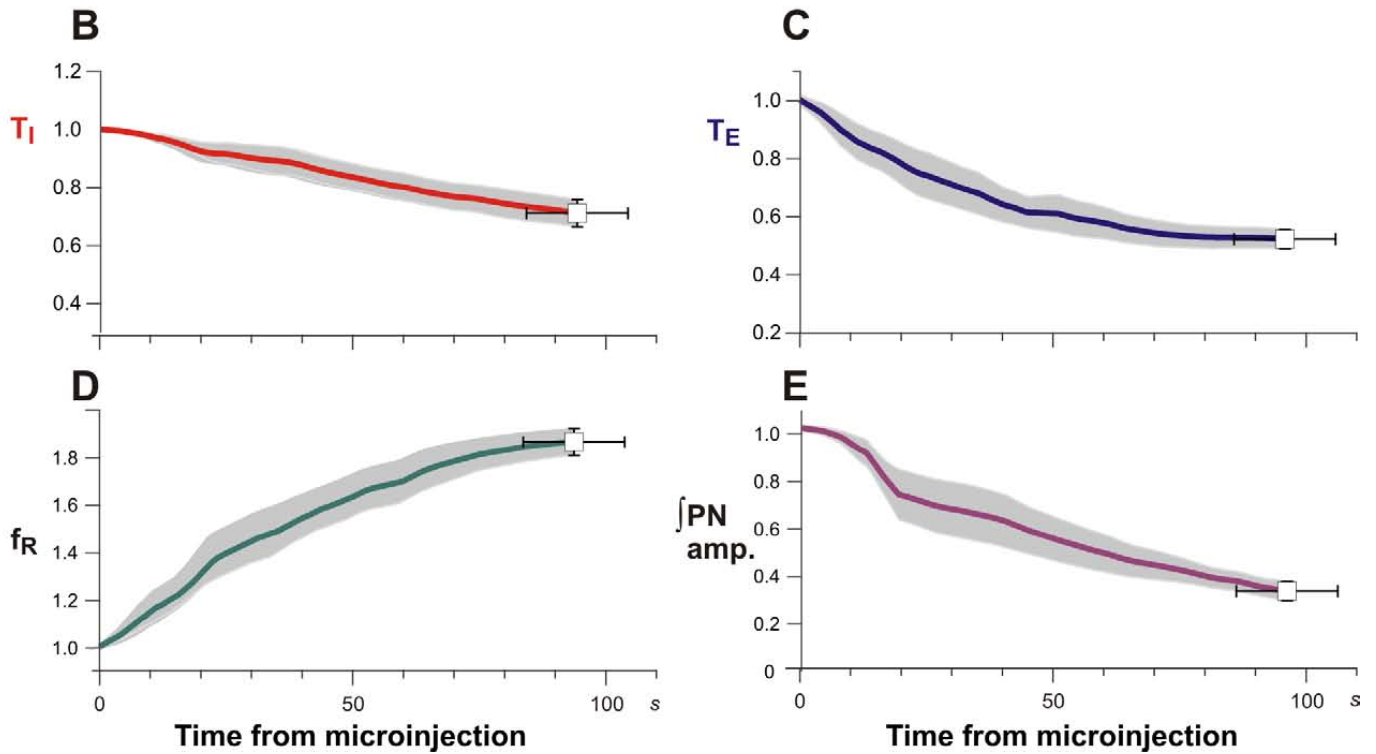


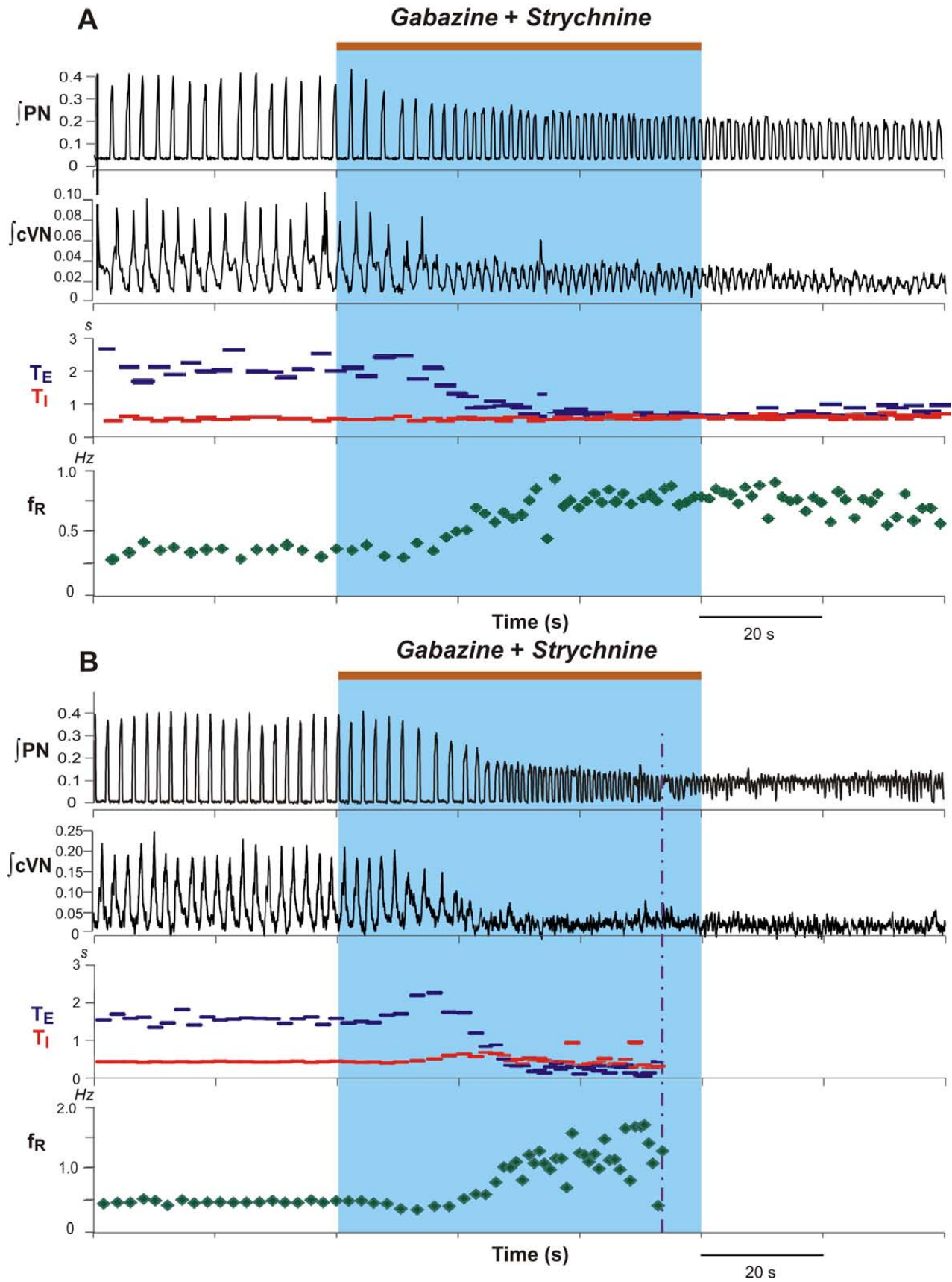


Gabazine + Strychnine in pre-BötC (*in vivo*)



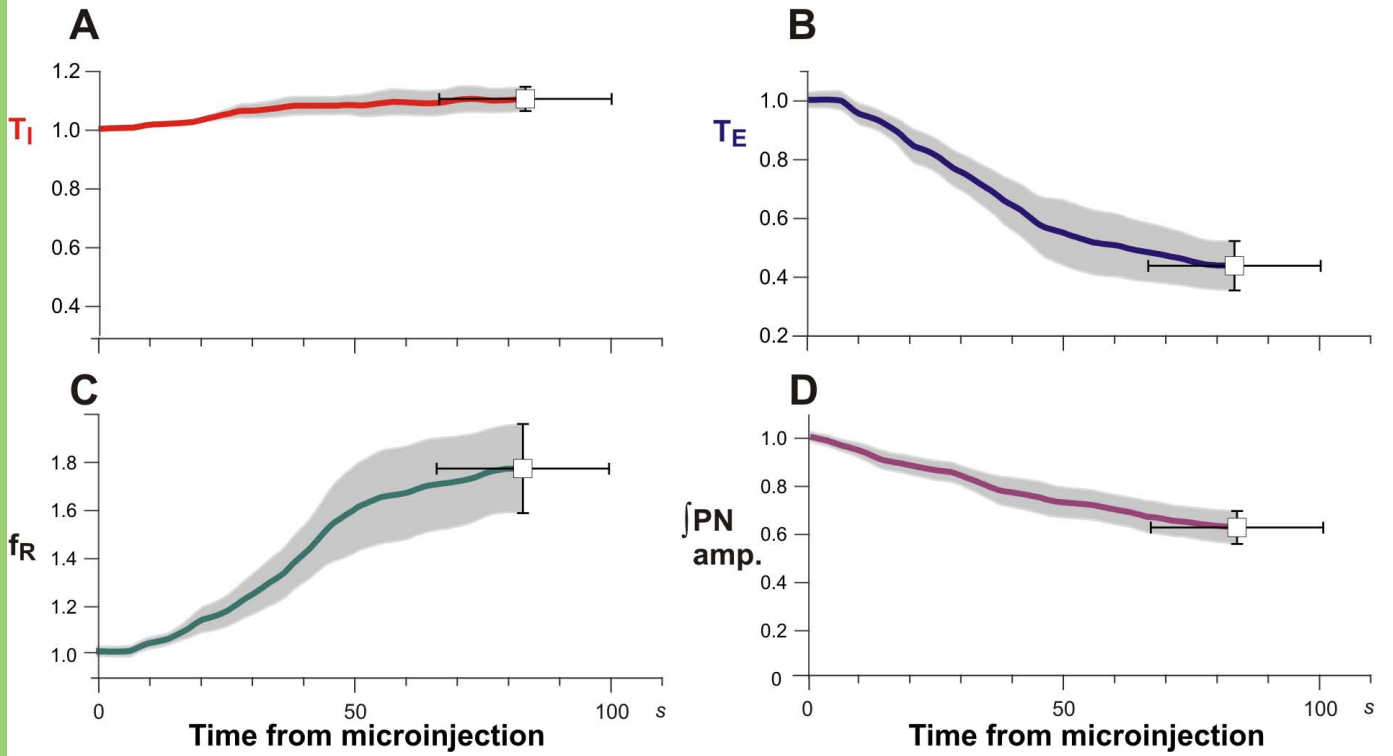
Normalized values ($n = 6$)



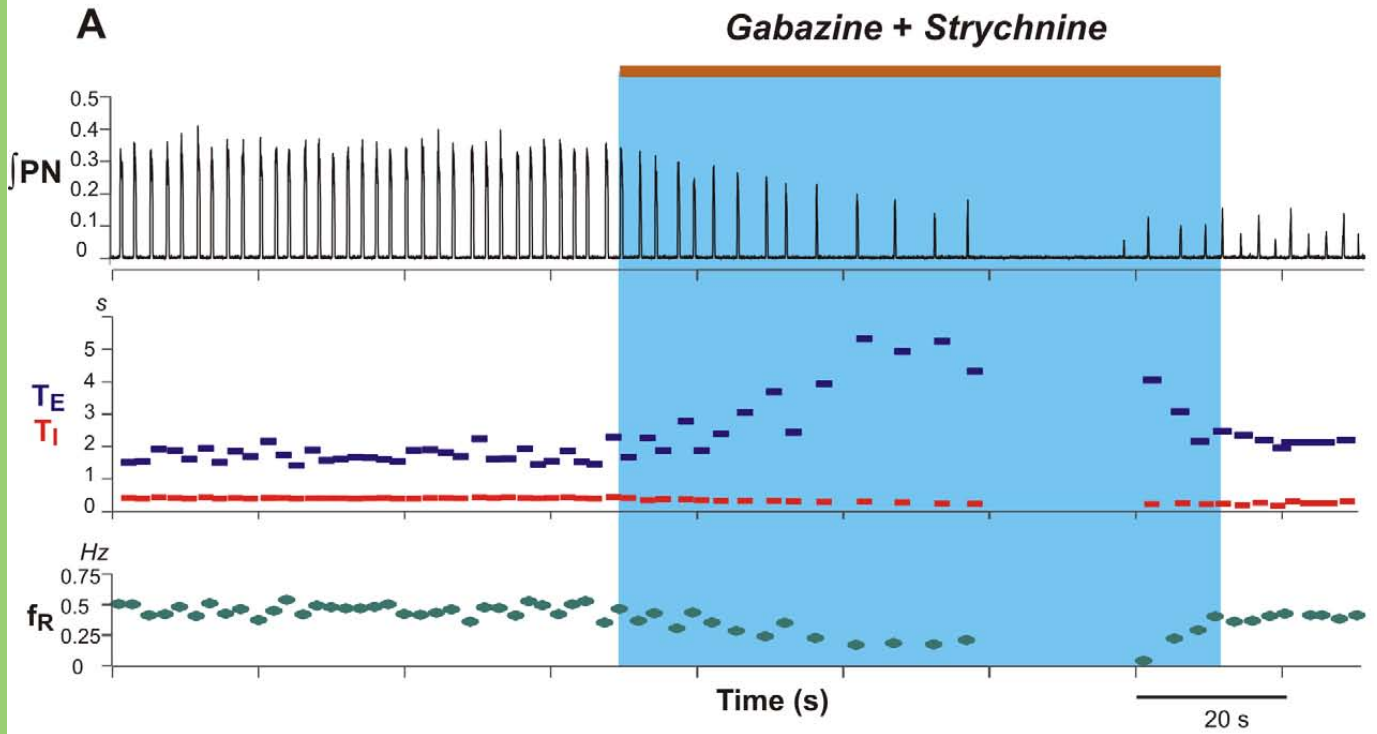
Gabazine + Strychnine in pre-BötC (*in situ*)

Gabazine + Strychnine in pre-BötC (*in situ*)

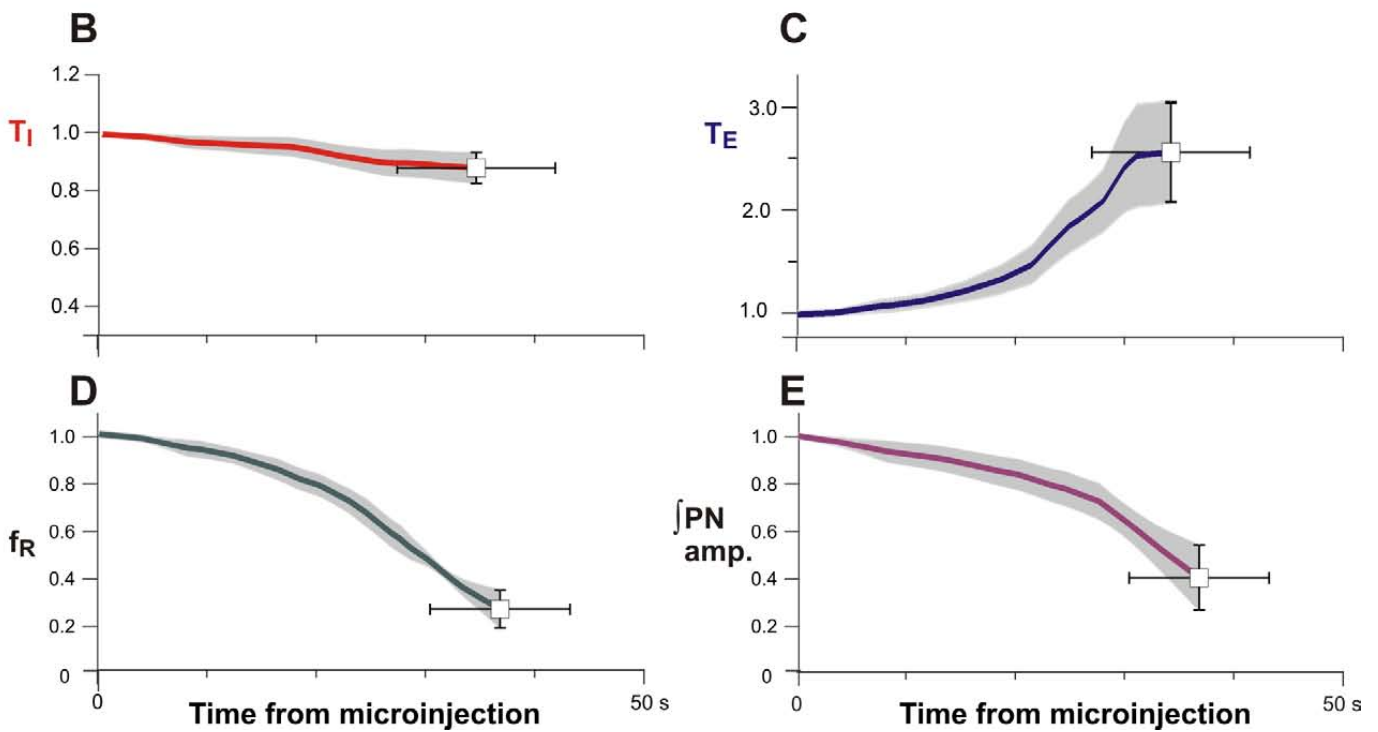
Normalized values ($n = 6$)



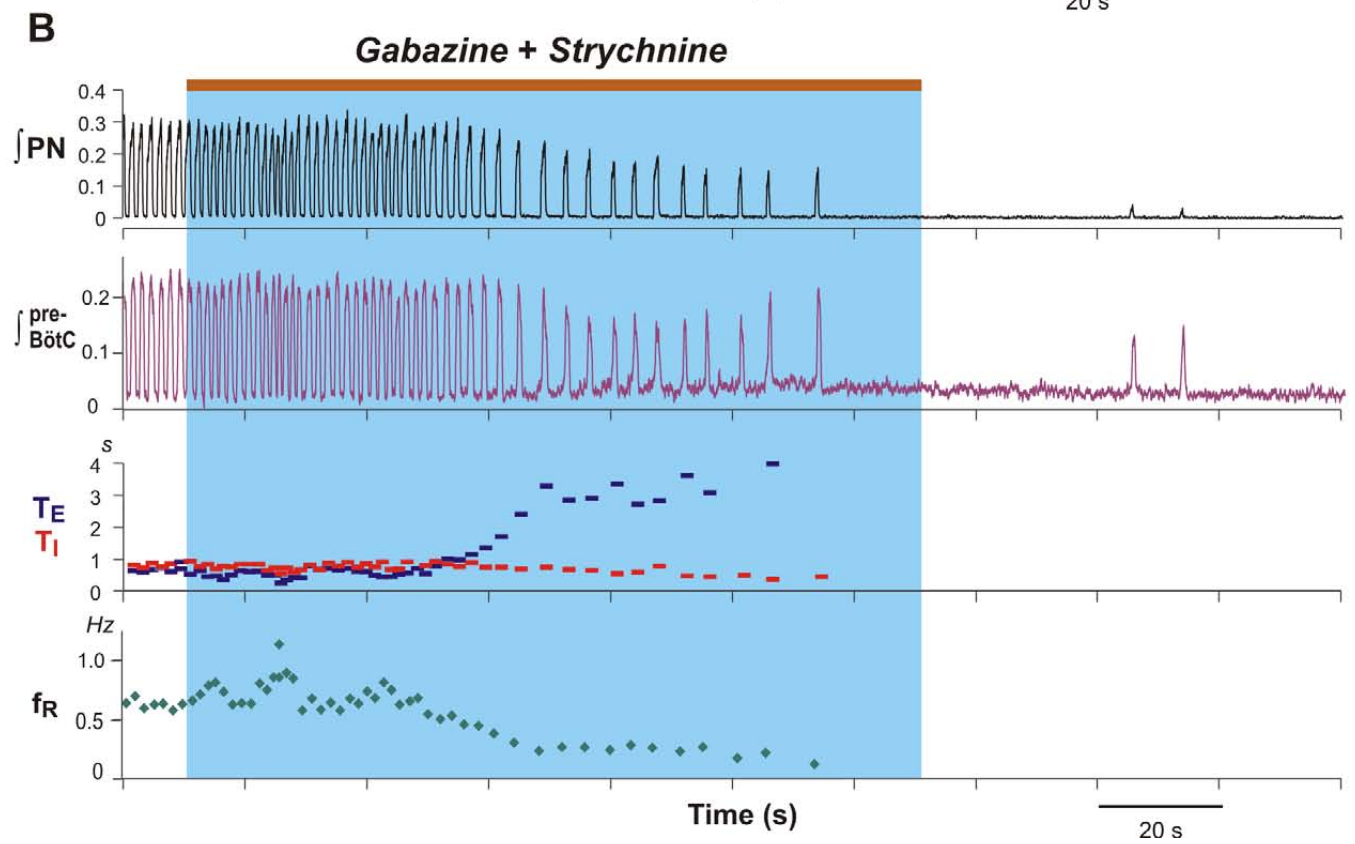
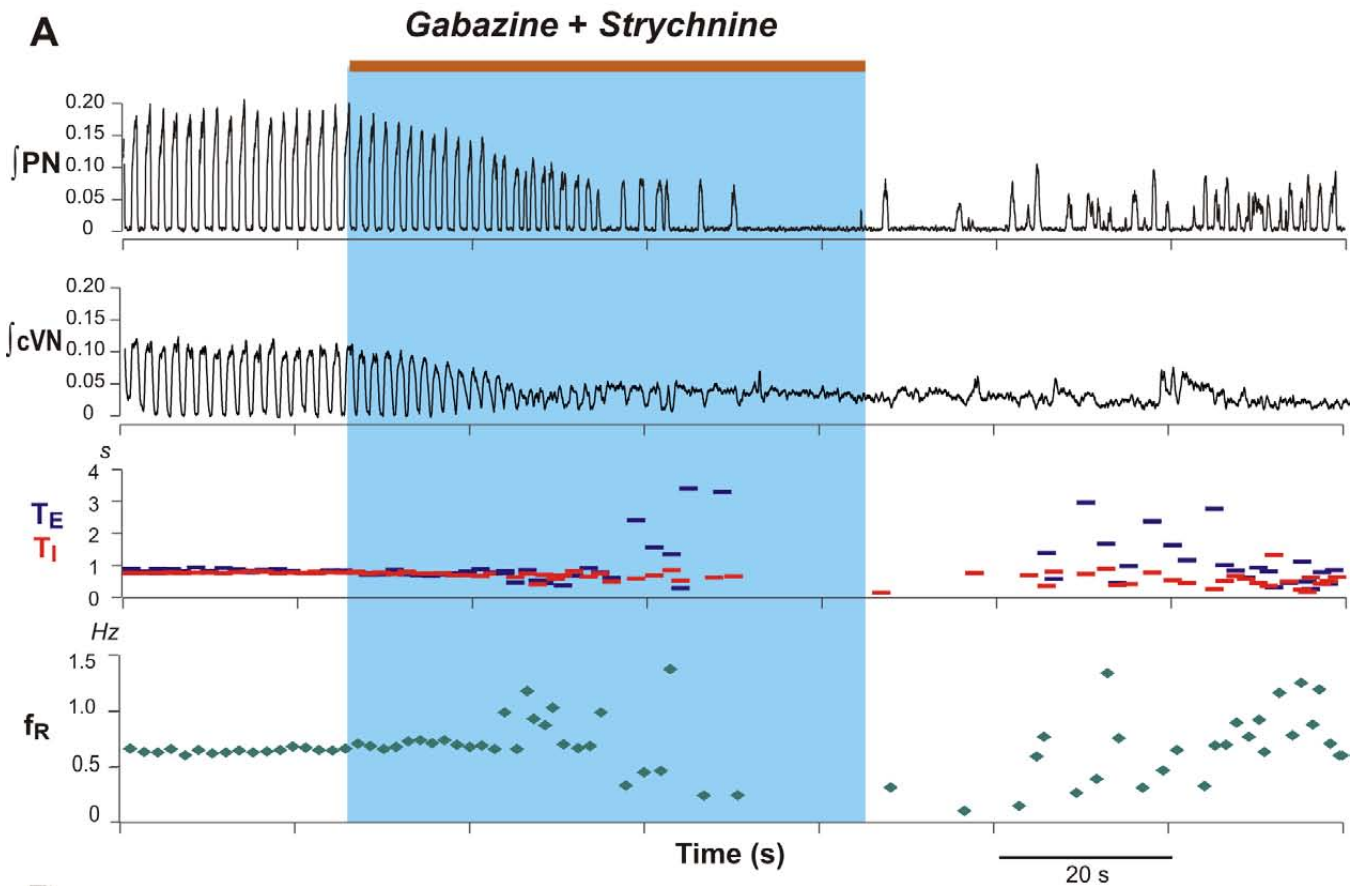
Gabazine + Strychnine in BötC (*in vivo*)

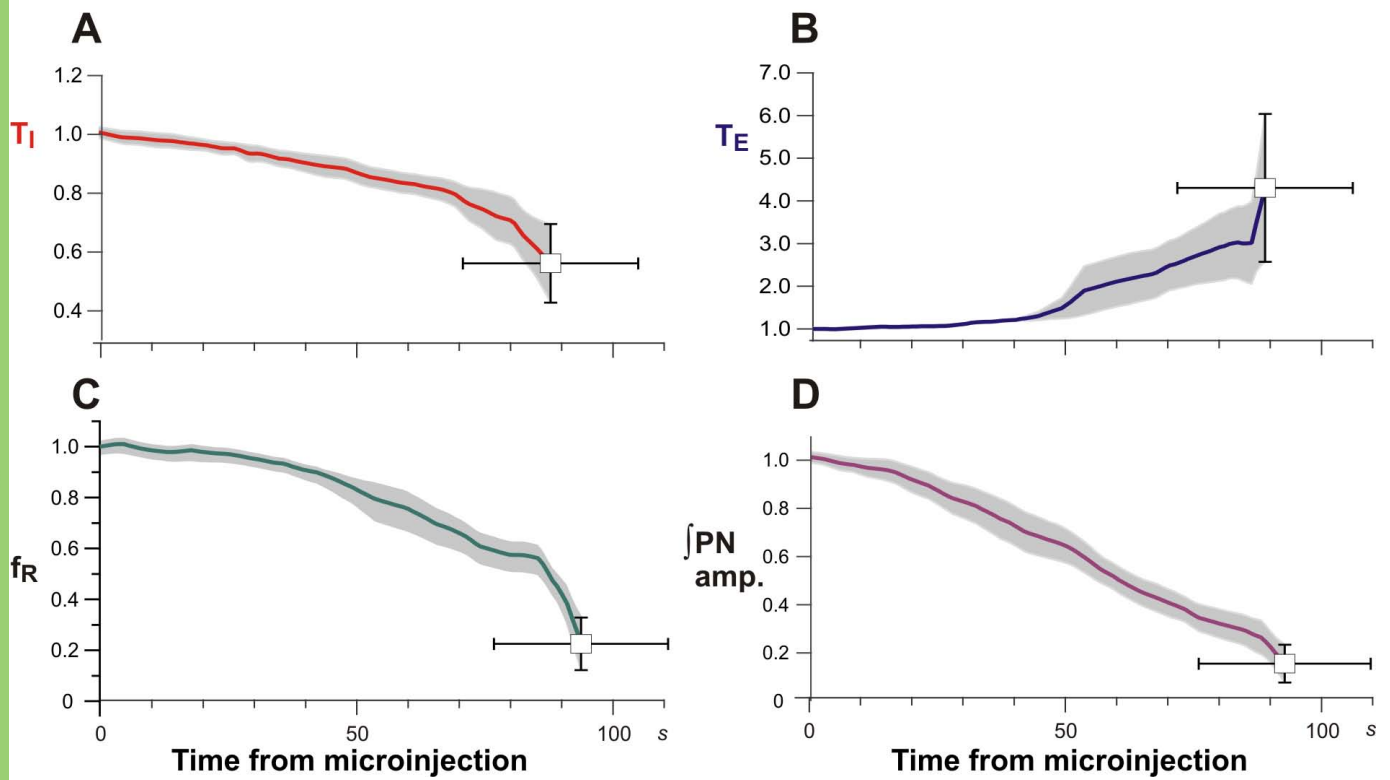


Normalized values ($n = 6$)

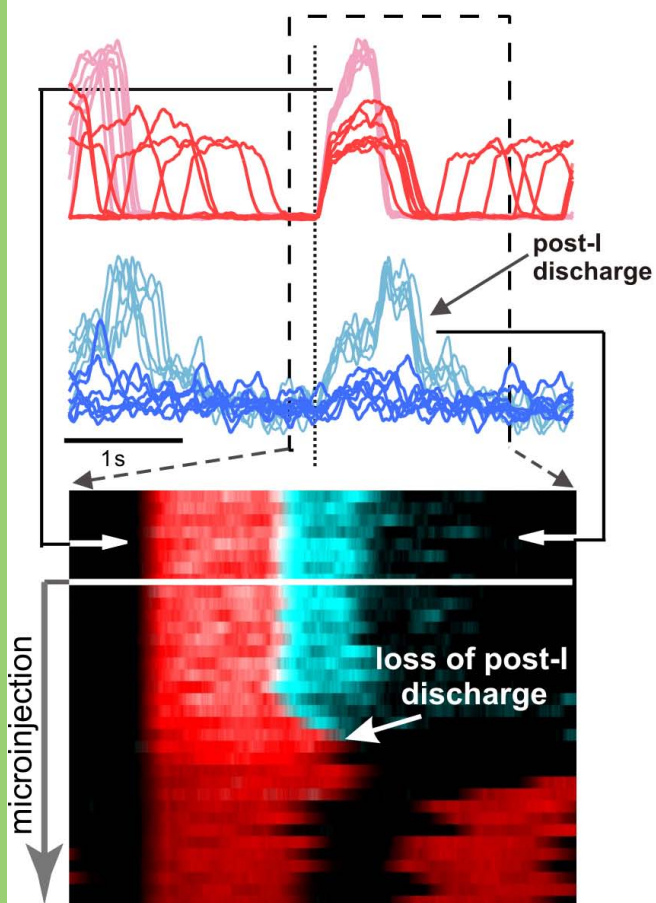


Gabazine + Strychnine in BötC (*in situ*)

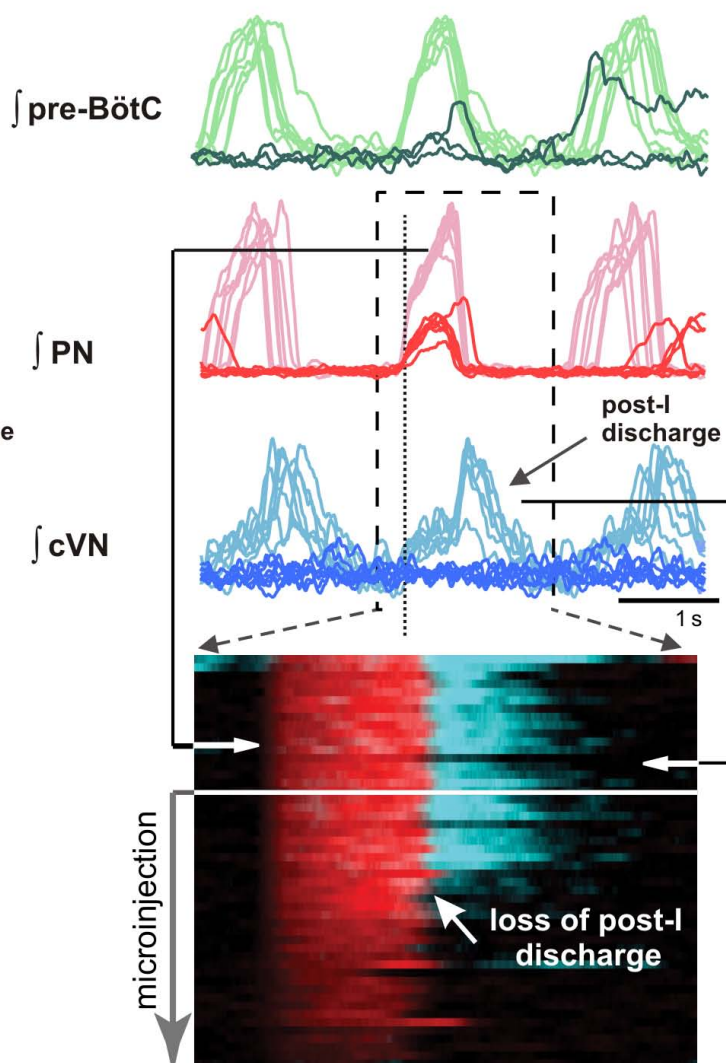


Gabazine + Strychnine in BötC (*in situ*)Normalized values ($n = 6$)

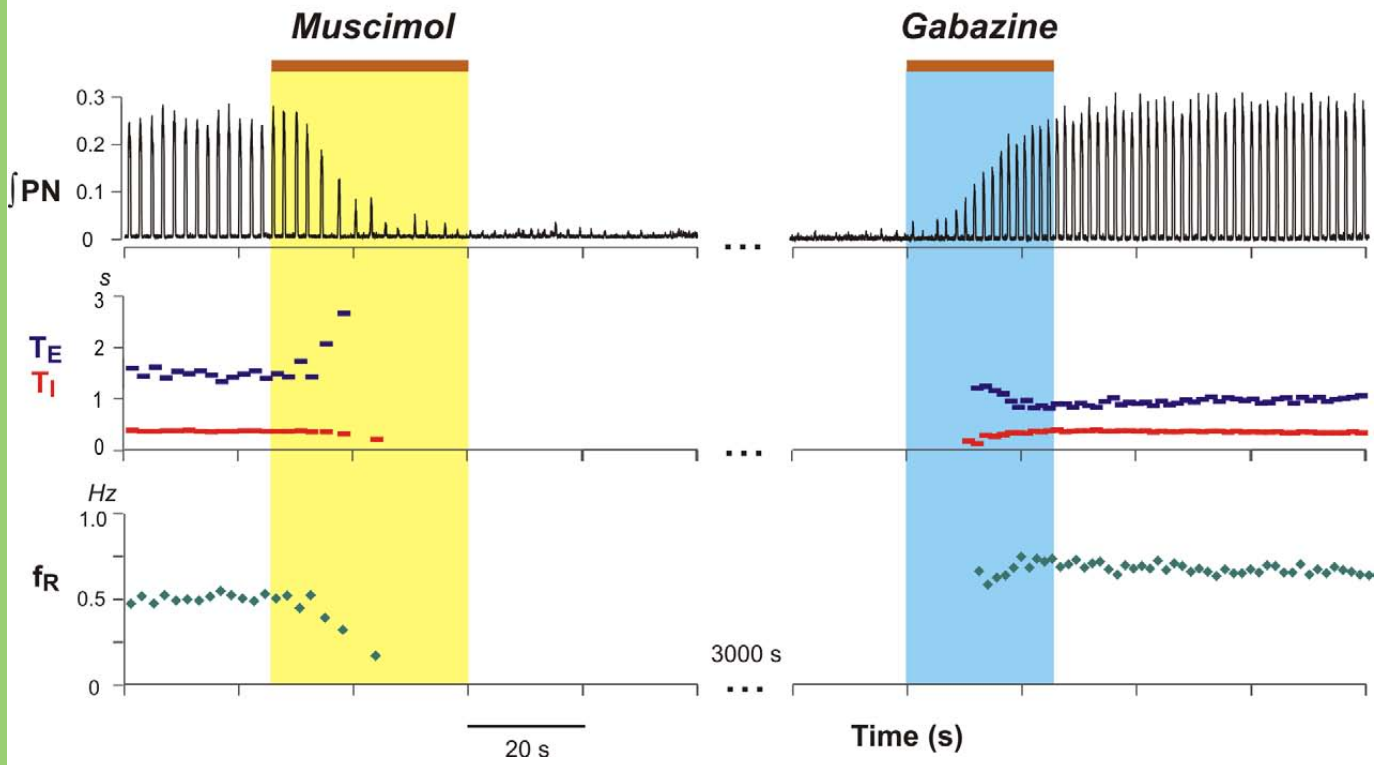
A Gabazine + Strychnine in pre-BötC (*in situ*)



B Gabazine + Strychnine in BötC (*in situ*)

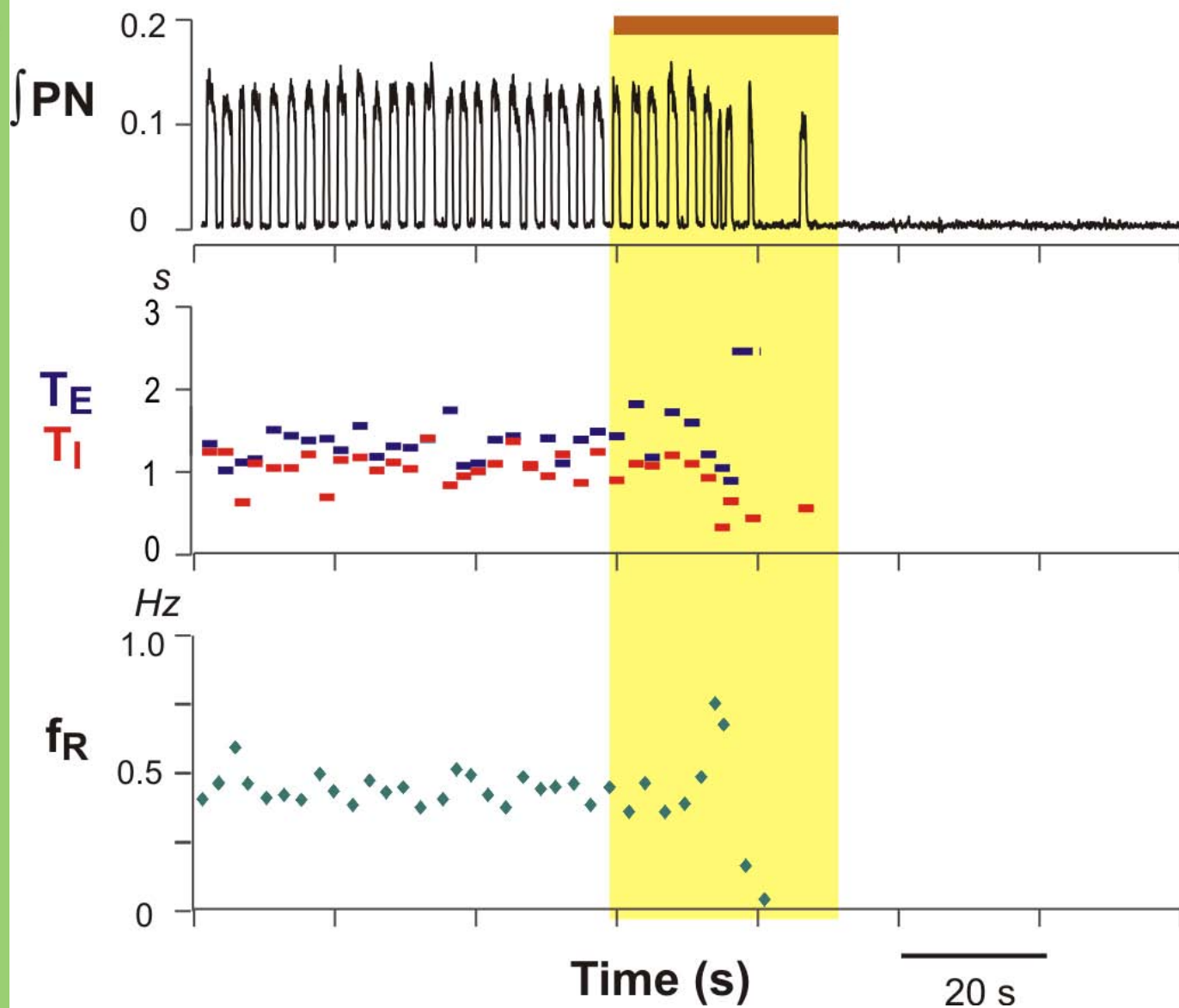


Muscimol in pre-BötC (*in vivo*)

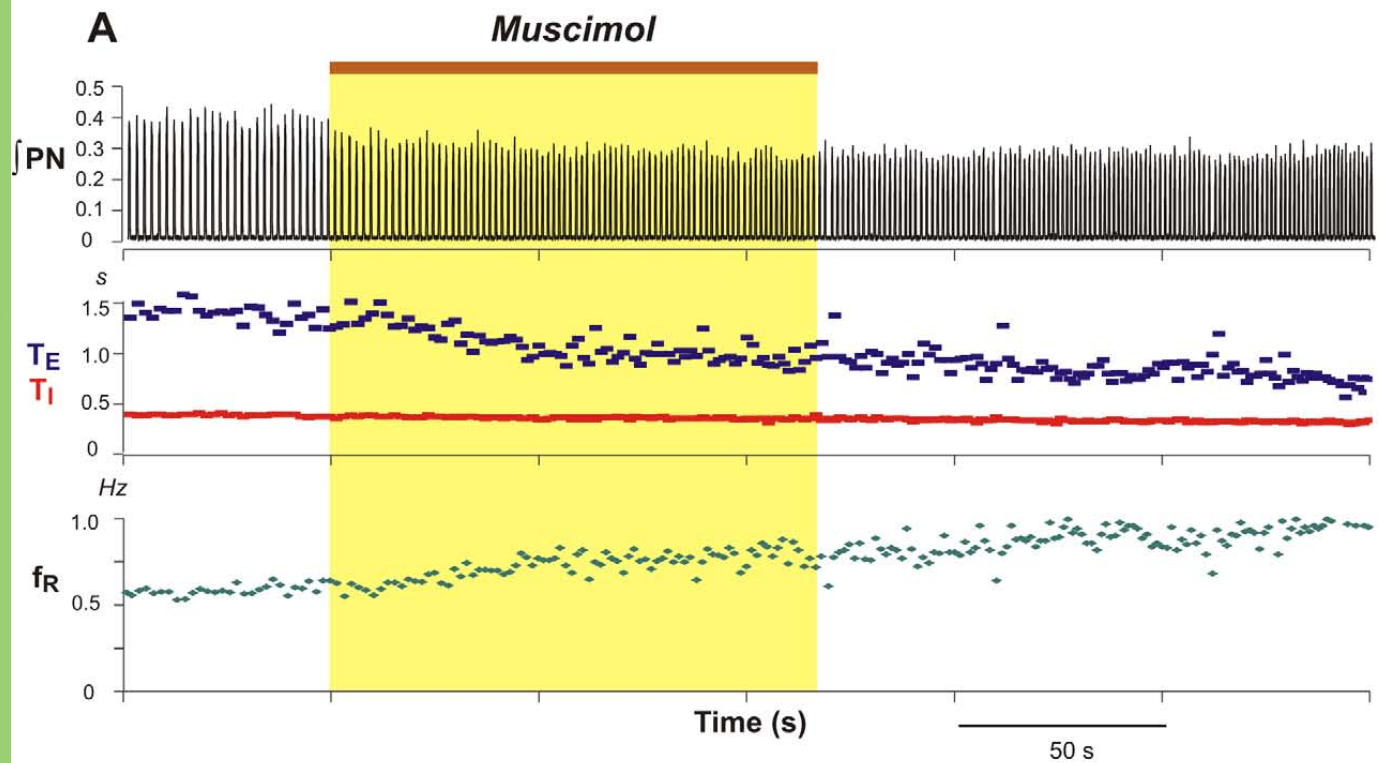


Muscimol in pre-BötC (*in situ*)

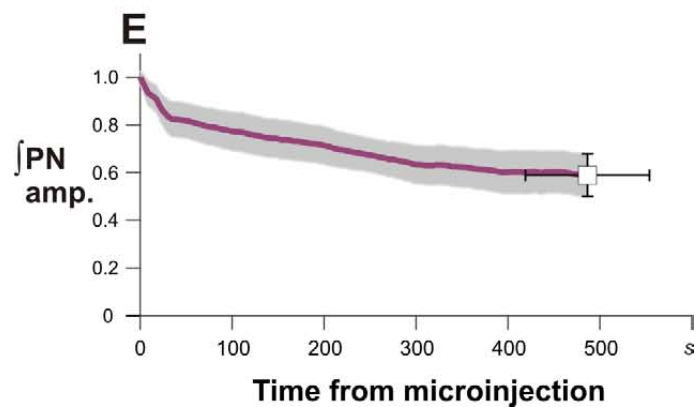
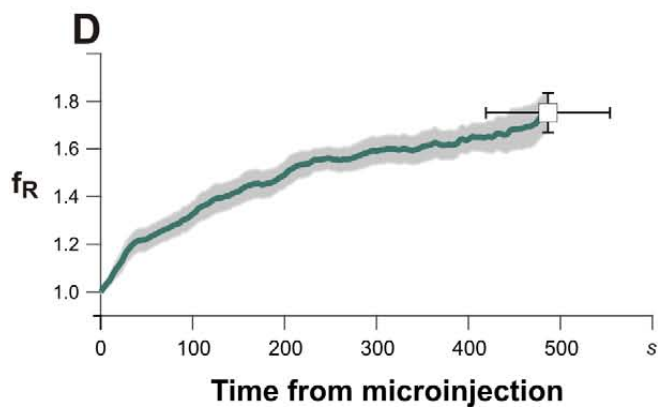
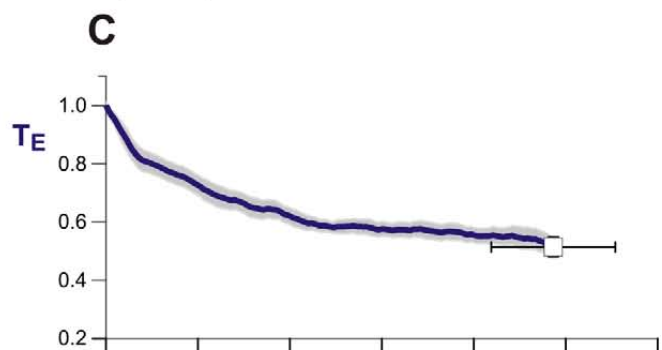
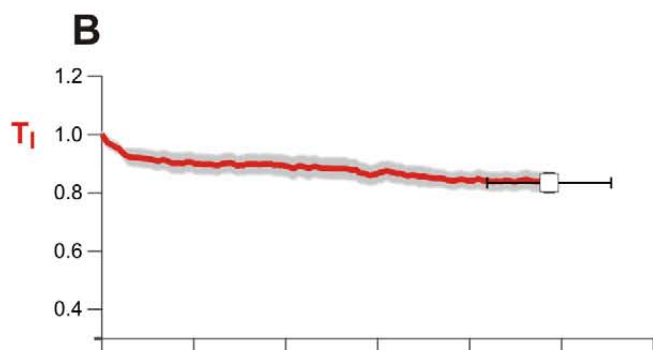
Muscimol



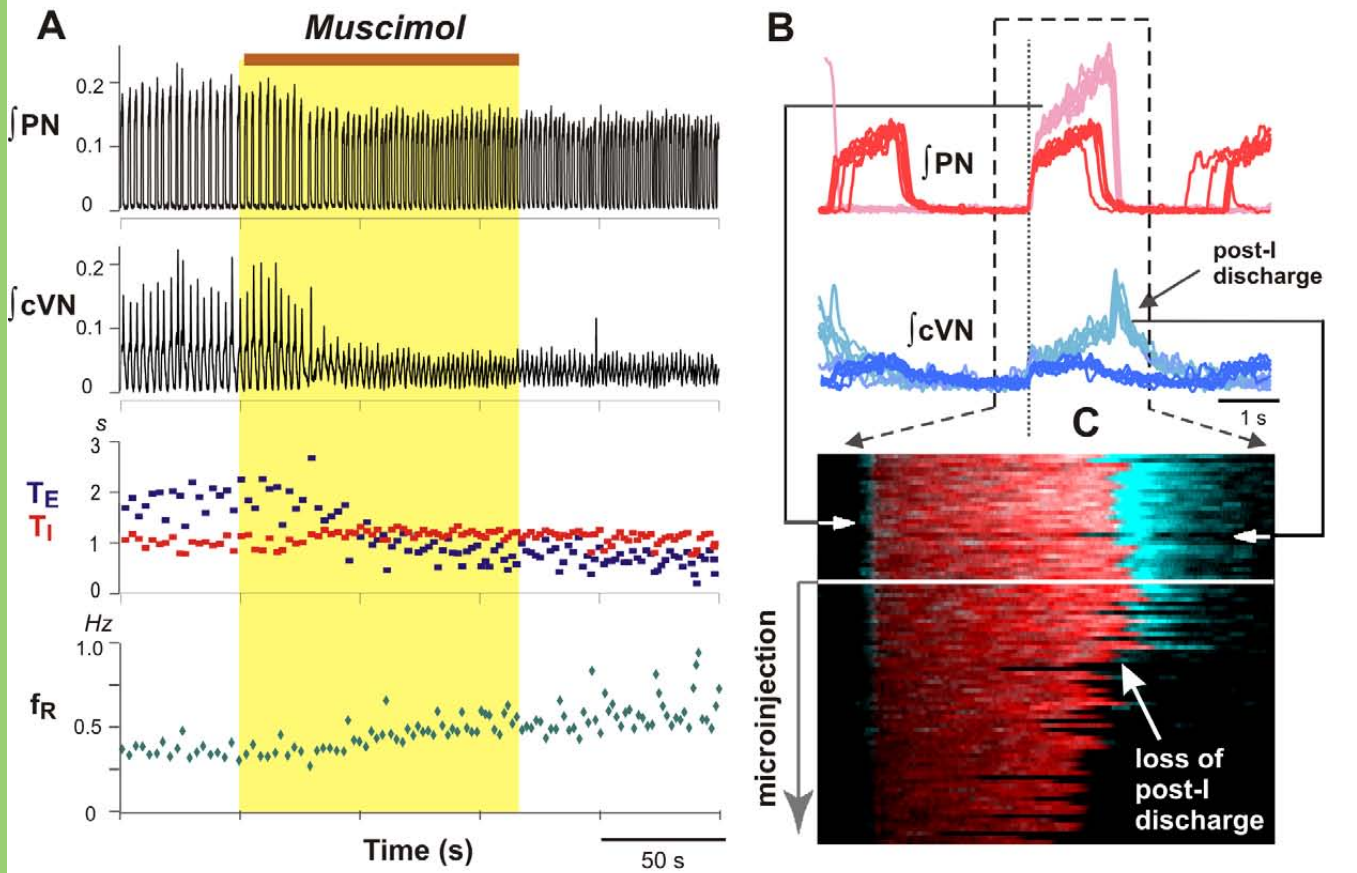
Muscimol in BötC (*in vivo*)



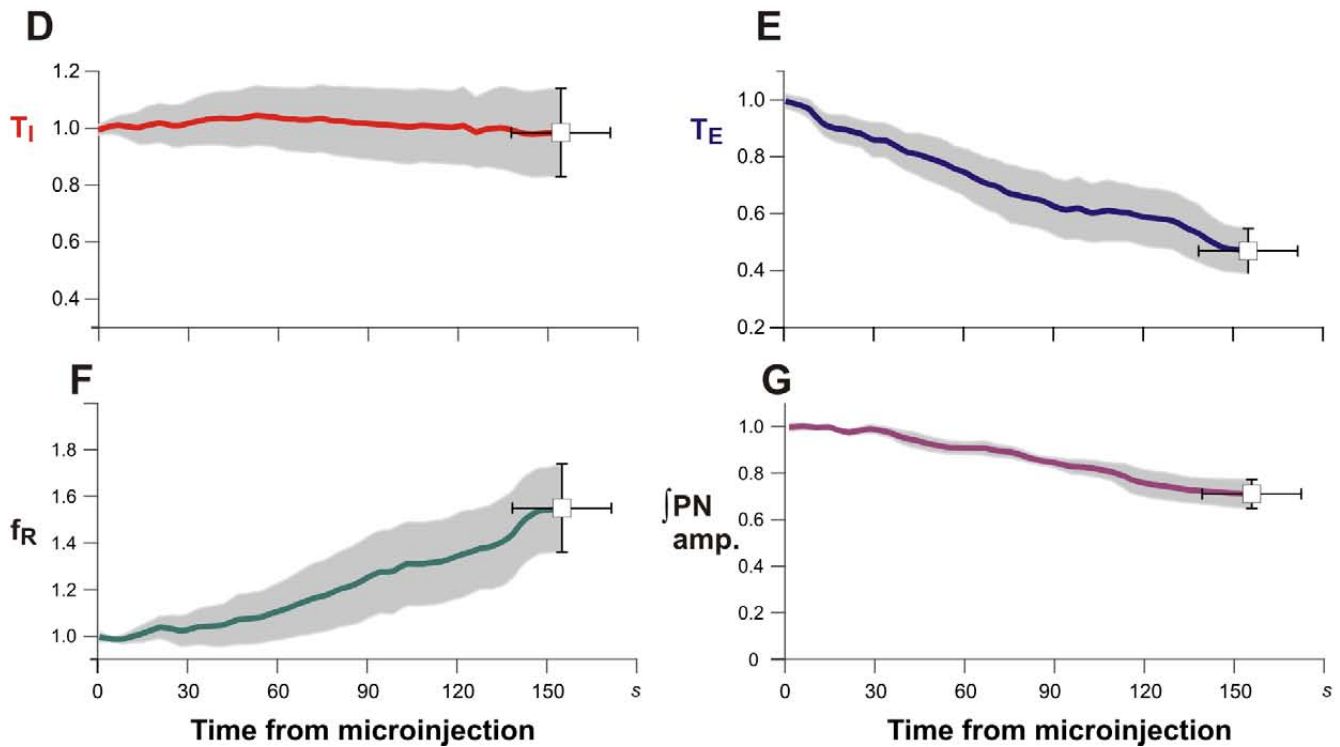
Normalized values (*n* = 7)



Muscimol in BötC (*in situ*)



Normalized values ($n = 5$)



Gabazine + Strychnine in BötC (*in vivo*)

Gabazine + Strychnine

